DOI: 10.26599/FSHW.2026.9251090

Contents lists available at SciOpen

Food Science and Human Wellness

journal homepage: https://www.sciopen.com/journal/2097-0765

China Food Publishing Co.

Choline as a Key Modulator of *Ganoderma Lucidum* Spore Oil in Preventing Pressure Overload-induced Heart Failure with Reduced Ejection Fraction

Weijiang Tan[1,2#], Shuang Zheng[2#], Honghua Chen[2], Xiang Li[2], Xuecong Ren[2], Jianxin Chen[1*], Feng Hua Yang[2*]

[1]*College of Veterinary Medicine, South China Agricultural University, Guangzhou, 510642, China.*

[2]*Guangdong Provincial Biotechnology Research Institute (Guangdong Provincial Laboratory Animals Monitoring Center), Guangzhou, 510663, China.*

ABSTRACT: Chronic pressure overload, caused by hypertension or aortic stenosis, drives maladaptive cardiac remodeling from concentric hypertrophy to eccentric hypertrophy and heart failure with reduced ejection fraction (HFrEF). Metabolic dysregulation is central to this process and its resultant dysfunction. *Ganoderma lucidum* spore oil (GSO) exhibits cardioprotective properties; however, the underlying mechanisms and key mediators remain unclear. This study aimed to determine whether GSO ameliorates pressure overload-induced HFrEF by modulating myocardial metabolism, and to identify specific metabolites mediating its effects. Male C57BL/6J mice underwent transverse aortic constriction (TAC) to induce progressive remodeling. Mice were randomized to sham operation (SHAM), TAC, TAC+GSO (100 mg/kg/day), or TAC+physiological dose choline (7 mg/kg/day), according to the experimental design, for up to 8 weeks. Left ventricular geometry, function (echocardiography and strain imaging), myocardial injury (cardiac troponin T assay and histology), bioenergetics (ATP and actomyosin MgATPase), Ca^{2+} handling, electrical activity (electrocardiogram and ion channel expression), and global metabolism (untargeted metabolomics) were assessed. GSO attenuated hypertrophy, fibrosis, and ejection fraction (EF) decline across the concentric-eccentric transition, and restored myocardial choline depleted by TAC. Low-dose choline supplementation reproduced the benefits of GSO on systolic and diastolic function, deformation indices, myocardial structure, conduction stability, ATP content, Ca^{2+} handling, and MgATPase activity. Transcriptomics and pathway analysis (RNA sequencing and Ingenuity Pathway Analysis) mapped signaling changes. Mechanism study verified that both interventions suppressed pro-hypertrophic signaling by reducing phosphorylation along the RAF/MEK/ERK cascade. Myocardial choline preservation is a central mechanism of GSO-mediated cardioprotection against pressure overload-induced HFrEF. Physiological choline restoration recapitulates these benefits, defining a novel metabolic–signaling axis with translational potential in hypertensive heart disease.

Keywords: Ganoderma lucidum; Choline; Heart failure; Pressure overload; Hypertrophy; Metabolism

1. Introduction

Heart failure (HF) remains a global health challenge, affecting over 56.2 million individuals across 204 countries in 2019, with hypertension being a leading risk factor accounting for approximately 20% of newly

[#]Weijiang Tan and Shuang Zheng contributed equally to this work and share first authorship.
***Corresponding author**
jxchen@scau.edu.cn; fenghua.yang@gdlami.com

Received 24 January 2025
Received in revised from 6 March 2025
Accepted 3 April 2025

reported HF cases [1]. Approximately 31% of adults worldwide have hypertension, which is defined as systolic blood pressure (SBP) ≥ 140 mmHg, diastolic blood pressure (DBP) ≥ 90 mmHg, or use of antihypertensive medication [2]. Sustained systemic hypertension imposes chronic pressure overload of the left ventricle (LV), increasing wall stress and initiating a cascade of molecular and structural changes. The LV initially undergoes adaptive concentric remodeling/hypertrophy that preserves ejection fraction (EF) but promotes diastolic dysfunction, predisposing susceptible individuals to HF with preserved ejection fraction (HFpEF). With persistent overload and additional myocardial injury, maladaptive remodeling with chamber dilation (an eccentric pattern) may ensue, leading to reduced EF and HFrEF [3-5].

Given the complexity and progression of hypertension-induced cardiac remodeling, it becomes clear that early intervention is critical to prevent the transition from compensatory changes to maladaptive remodeling. We previously used a transverse aortic constriction (TAC) mouse model to mimic hypertension-induced structural and functional alterations of the heart. In this model, TAC-induced pressure overload initially causes concentric hypertrophy accompanied by an increased EF. This is followed by a transitional phase characterized by pseudonormal internal dimensions and preserved EF. Prolonged pressure overload, however, culminates in ventricular dilation with reduced EF [6]. Indeed, all forms of cardiac remodeling induced by pressure overload, including concentric hypertrophy, pseudonormal remodeling, and eccentric hypertrophy, are detrimental to cardiac function. Particularly, cellular hypertrophy and loss, inflammation, fibrosis, disrupted electrical conduction, altered metabolism, and impaired contractility are commonly observed [7-9]. Current therapies for HFrEF (including angiotensin-converting enzyme inhibitors/angiotensin II receptor blockers, β-blockers, mineralocorticoid receptor antagonists, and sodium-glucose cotransporter 2 inhibitors) primarily target the neurohormonal or hemodynamic pathways. However, these agents incompletely address central injury mechanisms, notably mitochondrial energy failure, metabolic substrate imbalance, oxidative stress, inflammation, and fibrosis. Moreover, these agents rarely reverse established maladaptive remodeling or restore lost contractile reserve. Thus, therapies that can intervene at an earlier stage of cardiac remodeling, particularly those that target the metabolic disturbances that underlie these pathophysiological processes, are urgently required. Therefore, developing therapies that intervene upstream at the level of metabolic pathology while providing structural protection remains a critical unmet need.

Natural products with multi-targeted bioactivity, such as *Ganoderma lucidum* spore oil (GSO), are attractive therapeutic candidates. *G. lucidum*, an edible medicinal mushroom that has long been used in East Asian medicine for cardiovascular ailments, produces spore oil containing triterpenes, unsaturated fatty acids, polysaccharides, and sterols. These constituents have been reported to possess antioxidative, anti-inflammatory, and metabolism-regulating properties [10-12]. Experimental studies have shown that Ganoderma-derived preparations lower systolic and diastolic blood pressure in the rabbit and rat models [13], including genetically hypertensive rats [14, 15]. GSO also prevents cardiac dysfunction in a pressure overload mouse model that mimics hypertensive heart disease [16].

Based on these findings, GSO holds promise in addressing the underlying metabolic disturbances associated with hypertension-induced HF. Furthermore, the cardioprotective effects of *G. lucidum* are increasingly recognized as being closely associated with its regulation of metabolic processes. For instance, *G. lucidum* spore extracts reduce aortic plaque formation in rabbits with high-fat diet-induced hyperlipidemia [17], and decrease total cholesterol in rats with trimethylamine N-oxide (TMAO)-induced cardiac dysfunction [18]. In aged rats, *G. lucidum* enhances mitochondrial enzyme activities and the function of respiratory chain complexes in the heart [19]. However, the exact molecular mediators responsible for these effects remain unclear.

This raises the intriguing possibility that GSO might offer therapeutic benefits beyond its antioxidative and anti-inflammatory properties, particularly through the regulation of heart-specific metabolic pathways. Hypertension and pressure overload frequently coexist with systemic metabolic disturbances, including hyperlipidemia, insulin resistance, and diabetes, which worsen myocardial energetics [20, 21]. Choline metabolism occupies a central metabolic nexus: it supports membrane phospholipid synthesis (e.g., phosphatidylcholine), acetylcholine neurotransmission, and one-carbon methylation cycles [22, 23]. Choline deficiency links to impairment of cardiac function, while supplementation at physiological doses improves cardiac injury in animal models [24, 25]. Conversely, excessive choline intake may promote gut microbiota–derived TMAO, which is associated with heightened risk of cardiovascular diseases [26]. Given the growing recognition of the role of metabolic dysregulation in hypertension-induced HF, the potential impact of GSO on myocardial choline homeostasis in the context of pressure overload represents an important area of exploration. Whether the cardioprotective effects of GSO involves preservation of myocardial choline homeostasis under pressure overload has not been investigated.

Therefore, we aimed to evaluate the impact of GSO on LV remodeling and function during the hypertrophic transition in TAC mice, employ untargeted metabolomics to identify myocardial metabolites altered by pressure overload and restored by GSO, assess whether direct supplementation of candidate metabolites can reproduce the benefits of GSO, and elucidate the overlapping and distinct molecular pathways that are affected by GSO and the key metabolite.

2. Materials and methods

2.1 Animals and experimental design

Male mice (C57BL/6J; 3 months old) were housed in a specific pathogen-free, AAALAC-accredited (File No. 001469, 2022) and licensed (No. SYXK(YUE)2021-0122) facility at the Guangdong Provincial Biotechnology Research Institute (formerly known as the Guangdong Laboratory Animal Monitoring Institute). The ambient conditions were maintained at 24 ± 2 ℃ with a humidity level of 40–60% and a 12-h light/dark cycle. All animal experiments were conducted according to the guidelines of the Institutional Animal Care and Use Committee (Plan No: IACUC2021716).

TAC was performed to induce LV pressure overload. GSO (100 mg/kg body weight, by oral gavage) was administered once daily, starting 3 days after surgery, and continued for 8 weeks. Prior to selecting the 100

mg/kg dose, three doses (50, 100, and 150 mg/kg) were evaluated in a pilot study (Fig. S1). After 8 weeks of TAC-induced pressure overload, cardiac structure and function were assessed (echocardiography for LV geometry and systolic/diastolic indices). Experimental groups at this stage included SHAM (sham operation + 0.9% NaCl), TAC (TAC + 0.9% NaCl), and TAC+GSO. Following the prediction of a specific metabolites modulated by GSO under pressure overload using untargeted metabolomics, an additional TAC+CHO group was added, in which the candidate metabolite choline (7 mg/kg body weight, Cat. No. C7527, Sigma-Aldrich, St. Louis, MO, USA) was administered intraperitoneally to bypass the microbiota-dependent pathway. Next, cardiac remodeling, ventricular wall motion, and global cardiac function; as well as on electrical activity, myocardial fibrosis, and myocardial contractility in hearts with pressure overload. Fibrosis was assessed by Masson's trichrome staining, and myocardial contractility was analyzed using isolated myocytes and myofilaments.

To elucidate intracellular signaling, we first performed RNA sequencing (RNA-seq) and followed this with Ingenuity Pathway Analysis (IPA, QIAGEN). We then verified the expression of key proteins through immunoblotting in both in vivo and in vitro models. Finally, the magnitude and spectrum of effects elicited by individual metabolites were compared with those of GSO to determine whether this metabolite mediates the cardioprotective actions of GSO in pressure-overloaded hearts.

2.2 Analysis of GSO composition

GSO, provided by Guangdong Yuewei Edible Fungi Technology Co., Ltd. (as described previously [16]), was analyzed for its volatile composition and ganoderic acid content.

Gas chromatography–time-of-flight–mass spectrometry (GC-TOF-MS) was performed to analyze the volatile constituents of GSO. Extracts were first subjected to methoxyamination (30 ℃, 90–120 min) and then silylated with MSTFA containing 1% TMCS (37.5 ℃, 60 min). Derivatized samples (1 μL, splitless; injector 270 ℃; purge on at 0.75 min) were injected into an Agilent 7890B GC (Agilent Technologies, Santa Clara, CA, USA) coupled to a LECO TOF MS (LECO, St. Joseph, MI, USA) equipped with a DB-5MS capillary column (30 m × 0.25 mm i.d. × 0.25 μm film; Agilent Technologies, Santa Clara, CA, USA). Helium was used as the carrier gas at a constant flow of 1.0 mL/min. The oven program was: 80 ℃ (2 min), ramp at 12 ℃/min to 300 ℃, hold 8 min. Transfer line temperature was 270 ℃; ion source 220 ℃. Ionization was by electron impact (70 eV). Data were acquired in full-scan mode (m/z 50–500) at 25 spectra/s with a solvent delay of approximately 5 min. Raw data were processed in ChromaTOF software (v4.71, LECO) for baseline correction, noise reduction, smoothing, peak detection, spectral deconvolution, and cross-sample alignment. Putative compound identities were assigned by matching FAME-based retention indices and mass spectra against a local reference database (>1,000 in-house standards) supplemented with the LECO-Fiehn library.

The quantification of ganoderic acids was performed using high performance liquid chromatography (HPLC), in accordance with the Agricultural Industry Standard of the People's Republic of China (NY/T 2278-2012). Briefly, 1 g of GSO was weighed and dissolved in 5 mL of chromatographic-grade methanol, followed by ultrasonication for 25 min. The solution was filtered through a 0.45 μm membrane, evaporated to

dryness under a nitrogen stream, and reconstituted to 1 mL with methanol. Analysis was carried out on an octadecylsilyl (C18) column (4.6 mm × 250 mm, 5 μm). The mobile phase consisted of solvent A (0.05% phosphoric acid in water) and solvent B (acetonitrile) under a gradient elution program (identical to that used for calibration; detailed profile available upon request). The flow rate was 1.0 mL/min, the column temperature 30 ℃, the detection wavelength 258 nm, and the injection volume 10 μL. Ganoderic acids were quantified by external calibration using a standard curve generated from authentic ganoderic acid standards analyzed under identical chromatographic conditions.

2.3 TAC-induced ventricular pressure overload

TAC was used to induce LV pressure overload, leading to progressive cardiac remodeling and HF in mice, as previously described [6, 27]. In brief, after induction of anesthesia and endotracheal intubation, mice were mechanically ventilated with 1.5% isoflurane for maintenance. Following hair removal and skin disinfection, a longitudinal incision was made near the second rib to expose the transverse aorta. A blunt-ended, 26-gauge needle (approximately 1 cm long) was placed parallel to the aortic arch. A 7-0 suture was placed between the brachiocephalic trunk and left carotid artery and tied around the vessel and needle. After ligation, the needle was removed, and the chest was closed in layers. In the SHAM surgery group, thoracotomy was performed without aortic constriction.

2.4 Cardiac troponin T (cTnT) assay

Myocardial tissue cTnT levels were quantified in the experimental groups (SHAM, TAC, and TAC+GSO; n = 5–6 mice per group) using the Mouse Cardiovascular Disease Magnetic Bead Panel (Cat. No. MCVDMAG-77K, MilliporeSigma, Burlington, MA, USA) according to the manufacturer's instructions. Standard analyte dilutions were prepared serially. Heart tissue samples and controls were incubated with capture antibody-coated magnetic beads. Following the formation of immune complexes, biotinylated detection antibodies were added and incubated. After washing, phycoerythrin-conjugated streptavidin was added to generate the fluorescence signal. Fluorescence intensity was measured using a Luminex MAGPIX instrument (Luminex, Austin, TX, USA), and data were analyzed using the Milliplex Analyst software (MilliporeSigma).

2.5 Malondialdehyde (MDA) assay

For the SHAM, TAC, and TAC+GSO groups (n = 5–6 per group), myocardial tissue (0.2 g) was briefly rinsed in ice-cold saline, blotted dry, and homogenized in ice-cold 0.86% NaCl to obtain a 10% (w/v) homogenate. The homogenate was centrifuged at 1,150 × *g* for 15 min at 4 ℃, and the supernatant was collected. Protein concentration of an aliquot of the same supernatant was determined using a BCA assay kit (Cat. No. P0012, Beyotime Biotechnology, Shanghai, China), and MDA levels were measured using a commercial kit (Cat. No. A003-1, Nanjing Jiancheng Bioengineering Institute, Nanjing, China) following the manufacturer’s protocol. The absorbance was measured at 532 nm, and the MDA level was calculated from the corresponding standard curve.

2.6 Echocardiography

To investigate the impact of GSO and choline on cardiac morphology and function under pressure overload, an ultrasound imaging system equipped with a 30 MHz MS-400 probe (Vevo 2100; VisualSonics, Toronto, Canada) was used, as previously described [6, 27]. Briefly, mice from all experimental groups (SHAM, TAC, TAC+GSO, and, where applicable, TAC+CHO; n = 7–8 per group) were anesthetized with 1.5% isoflurane, endotracheally intubated, and maintained on a heating pad with continuous electrocardiogram (ECG) monitoring. Two-dimensional (B-mode) images were acquired, including parasternal long-axis, short-axis, and apical four-chamber views of the heart. Subsequently, M-mode images were collected. From these images, several cardiac morphological parameters were measured at end-systole and end-diastole, including the interventricular septal thickness (IVSs and IVSd), internal diameter (LVIDs and LVIDd), and posterior wall thickness (LVPWs and LVPWd). Finally, cardiac functional parameters, such as EF, fractional shortening (FS), and other relevant metrics, were calculated based on these measurements.

2.7 Histological examination

Following treatment completion, whole hearts from all experimental groups (SHAM, TAC, TAC+GSO, and TAC+CHO; n = 5–6 mice per group) were harvested and processed for histological analysis. Tissues were fixed in 4% paraformaldehyde, embedded in paraffin, and sectioned at 4 μm thickness. Sections were subjected to the following staining procedures: (a) hematoxylin and eosin (H&E) staining (hematoxylin and eosin, Sigma-Aldrich); (b) Masson's trichrome staining (Weigert's hematoxylin, Biebrich scarlet–acid fuchsin, and aniline blue; Sigma-Aldrich); and (c) wheat germ agglutinin (WGA) staining with fluorescein-conjugated WGA (Invitrogen, Waltham, MA, USA) to delineate cardiomyocyte borders, with nuclei counterstained with 4′,6-diamidino-2-phenylindole (DAPI; Invitrogen). Histological sections were examined under a microscope. Fibrotic area (from Masson's trichrome) and cardiomyocyte cross-sectional area (from WGA) were quantified using ImageJ (NIH https://imagej.nih.gov/ij).

2.8 Untargeted metabolomics of cardiac tissue

Untargeted metabolomic analysis was performed on cardiac tissues from the SHAM, TAC, and TAC+GSO groups (n = 6 per group) to identify metabolites altered by GSO in pressure-overloaded hearts. Extracts were analyzed on an Agilent 1260 Infinity HPLC coupled to a Thermo Q-Exactive (Thermo Fisher Scientific, Waltham, MA, USA; positive and negative modes in separate runs) using an amide column (3.5 μm, 2.1 × 100 mm; Waters, Milford, MA, USA). The mobile phases consisted of (A) water mixed with 25 mM ammonium acetate and 25 mM ammonium hydroxide and (B) acetonitrile, with the column equilibrated initially at 90% B. The injection volume was 4 μL and flow rate was 0.4 mL/min. Mass spectrometry parameters were set as follows: auxiliary gas heater temperature, 400 °C; sheath gas flow, 40 arb; auxiliary gas flow, 13 arb; spray voltage, 3.5 kV; capillary temperature, 350 °C; S-lens RF level, 55. Data-dependent acquisition (DDA) consisted of full-scan MS1 (60–900 m/z) at a resolution of 70,000, maximum injection time 100 ms, and automatic gain control (AGC) target 3e6, followed by top 4 ddMS2 at a resolution of 17,500,

AGC target 2e5, maximum injection time 45 ms, isolation window 1.6 m/z, and stepped normalized collision energies (NCE) of 30, 40, and 50%.

Raw files were analyzed using Thermo Compound Discoverer 2.1 with an untargeted metabolomics workflow. Processing included retention time alignment, compound detection, gap filling, and background subtraction. Compounds were annotated using mzCloud (ddMS2) and ChemSpider (mass tolerance: 5 ppm; databases: BioCyc, HMDB, KEGG, LipidMAPS).

To statistically evaluate the annotated metabolites, comparative heatmaps were generated using MetaboAnalyst 4.0. To evaluate group differences (SHAM vs. TAC; TAC vs. TAC+GSO), Orthogonal partial least squares discriminant analysis (OPLS-DA) was performed with SIMCA 14.1. To identify key metabolites mediating TAC-induced remodeling and the cardioprotective effects of GSO, we applied stringent S-plot criteria to the models: VIP > 2, |p(corr)[1]| > 0.5, and |p[1]| > 0.25. Directional changes were defined as: (1) SHAM vs. TAC: TAC-upregulated (p(corr)[1] > 0.5 and p[1] > 0.25), TAC-downregulated (p(corr)[1] < -0.5 and p[1] < -0.25); (2) TAC vs. TAC+GSO: GSO-induced reversal (e.g., TAC-up → GSO-down with sign-flipped p(corr)[1] and consistent VIP > 2). The metabolite exhibiting maximal |Δp(corr)[1]| between TAC and GSO states was selected for functional validation.

2.9 Strain imaging

Speckle-tracking-based strain imaging (VevoStrain; VisualSonics, Canada) was performed on long-axis B-mode images to quantify LV wall motion and deformation in TAC mice treated with either GSO or choline (n = 6–7 per group) [28]. A complete cardiac cycle was isolated from the long-axis B-mode echocardiographic cine. Endocardial and epicardial borders of the left ventricle were contoured; the automatically generated epicardial border was subsequently adjusted manually to improve accuracy. This preprocessing permitted continuous speckle tracking of the myocardium across end-diastole, end-systole, and the following end-diastole to derive segmental motion trajectories. The LV was divided into six segments: anterior and posterior walls were each subdivided into basal, mid, and apical segments. Wall motion indices included displacement (cm), defined as the change in ventricular wall position throughout the cardiac cycle, and velocity (cm/s), expressed as peak systolic and diastolic velocities denoting the maximal rates of myocardial motion during contraction and relaxation. Myocardial deformation parameters included longitudinal and radial strain (%) as well as their corresponding strain rates (s^{-1}). Longitudinal strain was defined as the percentage change in segment length relative to the end-diastolic length (negative values during systole), whereas radial strain was defined as the percentage increase in wall thickness relative to end-diastole (positive values during systole).

2.10 Pulsed wave and tissue Doppler imaging

Pulsed-Doppler ultrasound imaging of the aortic arch proximal to the constriction site was performed to assess aortic pressure. The animal and transducer were positioned at predetermined angles, coupling gel was applied to the cervical region, and B-mode images were obtained to visualize the aortic arch clearly. Pulsed Doppler signals were then recorded at defined sampling locations for subsequent analysis.

As previously described, diastolic function in hearts from the SHAM, TAC, TAC+GSO, and TAC+CHO groups (n = 7 mice per group) was assessed via pulsed wave and tissue Doppler imaging (TDI) using the Vevo2100 system [6]. Briefly, pulsed-wave Doppler was used to record transmitral blood flow velocities across the mitral valve, specifically the early (E) and late (A) diastolic peak velocities (mm/s); whereas TDI was used to capture mitral annular motion velocities, specifically the early (e′) and late (a′) diastolic annular peak velocities (mm/s).

2.11 Electrocardiogram recording

Electrical activity in anesthetized mice from the SHAM, TAC, TAC+GSO, and TAC+CHO groups (n = 7 mice per group) was assessed *in vivo* using a PowerLab data acquisition system equipped with an ECG monitoring module (PowerLab PL3504; AD Instruments, New South Wales, Australia). Briefly, mice were positioned supine on a temperature-controlled operating table, and anesthesia was maintained with 1% isoflurane throughout the recording. Lead II ECG recordings were obtained by inserting the negative electrode subcutaneously into the right forelimb, the positive electrode into the left hind limb, and the ground electrode into the right hind limb. Measured ECG parameters included P-wave duration (reflecting atrial depolarization), QRS interval (representing ventricular depolarization), and corrected QT (QTc) duration (calculated from the QT interval, which represents the total time for ventricular depolarization and repolarization, adjusted for heart rate).

2.12 RNA sequencing and prediction of target pathways

RNA sequencing (RNA-seq) was performed on heart tissues from the SHAM, TAC, TAC+GSO, and TAC+CHO groups (n = 5 mice per group) to assess gene expression levels, following previously established protocols [27, 29]. Briefly, purified mRNA was fragmented, reverse-transcribed into double-stranded cDNA, and ligated with adapters to construct paired-end libraries. After PCR amplification and quality control, libraries were sequenced on an Illumina NovaSeq 6000 platform (Illumina, San Diego, CA, USA). Raw FASTQ reads underwent adapter trimming and filtering (removing low-quality reads or those with >5% unknown bases). Clean reads were aligned to the reference genome using HISAT2 (http://daehwankimlab.github.io/hisat2/), followed by gene-level read counting with featureCounts (http://subread.sourceforge.net/). RNA-seq library preparation, sequencing, and initial data processing were performed by Shanghai Applied Protein Technology (Shanghai, China).

After differential expression analysis, the results were uploaded to IPA (QIAGEN) to explore pathways potentially targeted by GSO in TAC hearts. Differentially expressed genes (DEGs) were defined as genes with |fold change (FC)| ≥ 1.5 and P-value < 0.05. DEGs with FC ≥ 1.5 were classified as upregulated, and those with FC ≤ -1.5 were classified as downregulated. The comparison "TAC vs. SHAM" was used to identify canonical pathways altered by pressure overload. Significantly enriched pathways were selected using a threshold of P-value < 0.001 (-Log10(P-value) > 3). Pathway activation states were inferred using IPA's activation Z-score algorithm; pathways with Z-score > 2 were considered activated, whereas those with Z-score < −2 were considered inhibited. To infer possible mechanisms of GSO action, the TAC-associated

pathways were then compared to those influenced by GSO-treated (TAC+GSO vs SHAM) and choline-treated (TAC+CHO vs SHAM) TAC hearts.

2.13 Protein extraction and immunoblotting

Western blotting was performed to evaluate pathway regulation in pressure-overloaded hearts following GSO treatment, as described previously [29-31]. Mouse hearts from the SHAM group, TAC group, GSO-treated group, and choline-treated group (n = 6 mice per group) were homogenized in cell lysis buffer (Cat. No. 9803, Cell Signaling Technology, Danvers, MA, USA) containing protease inhibitors and 1% Triton X-100. Phosphatase inhibitors were added to detect phosphorylated proteins. The homogenates were centrifuged (12,000 × *g*, 20 min, 4 ℃), and the resulting supernatants were subjected to immunoblotting. Protein samples were separated by 12% SDS-PAGE and transferred onto polyvinylidene fluoride (PVDF) membranes. Primary antibodies from Cell Signaling Technology against the following proteins were used (cat. nos. in parentheses): RAS (67648), RAF1 (53745), p-RAF (9427), MEK (9122), p-MEK (9154), ERK1/2 (4695), p-ERK1/2 (4370), and GAPDH (5174). The antibody-bound bands on the PVDF membrane were detected using a chemiluminescent horseradish peroxidase substrate. The density of the bands was analyzed using the ImageJ software (NIH https://imagej.nih.gov/ij).

2.14 Myocardial ATP content

Myocardial ATP content was quantified in the experimental groups (SHAM, TAC, TAC+GSO, and TAC+CHO; n = 6 mice per group) using a colorimetric ATP assay kit (Cat. No. A095-1-1, Nanjing Jiancheng) following the manufacturer's instructions, as previously outlined [27]. Briefly, the whole heart was weighed and homogenized in nine volumes of 0.86% saline solution (weight/volume ratio = 1:9). A portion of the homogenate was centrifuged at 1,150 × *g* for 10 min, and the supernatant was collected for protein concentration determination using a Bradford assay kit (Beyotime Biotechnology, Shanghai, China). The remaining homogenate was boiled for 10 min and then centrifuged again under the same conditions. The absorbance of the resulting supernatant was measured at 636 nm using a spectrophotometer (Ultrospec 2100, Biochrom, Cambridge, UK) for ATP quantification.

2.15 Isolation of adult mouse cardiomyocytes

Hearts isolated from the SHAM, TAC, TAC+GSO, or TAC+CHO mice (n = 5 per group) were retrogradely perfused via the aorta using a Langendorff perfusion system (AD Instruments). After briefly washing with perfusion solution (in mM: 130 NaCl, 5.4 KCl, 0.4 NaH_2PO_4, 0.5 $MgSO_4$, 30 taurine, 0.01 BDM, 25 HEPES, 22 glucose, and 0.4 EGTA, pH 7.4), hearts were digested with 0.2 mg/mL protease type XIV (Cat. No. abs9154, Absin Biotechnology, Shanghai, China) and 1 mg/mL collagenase II (Cat. No. LS004176, Worthington Biochemical, Lakewood, NJ, USA) in perfusion solution containing 0.3 mM $CaCl_2$ and 2 mg/mL bovine serum albumin (BSA) for 10–12 min until swollen and pale. Hearts were minced, then digested further for 6 min at 37 ℃. Digestion was terminated by switching to the perfusion solution supplemented with 1.5 mM $CaCl_2$ and 10% fetal bovine serum (pH 7.4). The liberated cells were suspended

in modified Tyrode's solution (in mM: 140 NaCl, 5.4 KCl, 0.39 NaH_2PO_4, 0.5 $MgSO_4$, 5 HEPES, 5.5 glucose, and 1.8 $CaCl_2$, pH adjusted to 7.4 with NaOH) containing 0.2% BSA (Sigma-Aldrich) and 1% (v/v) penicillin-streptomycin (Yeasen Biotechnology, Shanghai, China).

2.16 Sarcomere length and calcium transient measurements

Sarcomere shortening and calcium transients were recorded in isolated adult mouse cardiomyocytes (prepared as in Section 2.15) using the IonOptix system (FSI800-0FT200Plus, IonOptix, Westwood, MA, USA). Cells were loaded with 4 μM Fluo-4 AM (Cat. No. 40704ES72, Yeasen Biotechnology) in Hanks' Balanced Salt Solution (HBSS; in mM: 137 NaCl, 0.35 Na_2HPO_4, 5.36 KCl, 0.44 KH_2PO_4, 0.81 $MgSO_4$, 1.26 $CaCl_2$, 4.17 $NaHCO_3$, 5.55 glucose) at 37 ℃ for 20 min in the dark. After loading, cells were washed and incubated in the same HBSS for 20 min at room temperature to allow complete de-esterification. Myocytes were field-stimulated at 1 Hz (10 V). Rod-shaped, quiescent myocytes were selected for recording. The chamber was perfused with warm (37 ℃) Tyrode's solution (as in Section 2.15). Sarcomere length was measured in real-time by tracking the diffraction pattern along the myocyte. Calcium transients were measured using Fluo-4 fluorescence. Data were acquired and analyzed using IonWizard 6.2.

2.17 Actomyosin MgATPase activity assay

Actomyosin (a complex of actin and myosin filaments) functions as an enzymatic catalyst for ATP hydrolysis, releasing energy that drives myofilament conformational changes during muscle contraction. We assessed MgATPase activity in myofilaments isolated from the SHAM, TAC, TAC+GSO, and TAC+CHO groups (n = 6 mice per group) using a modified protocol [32, 33]. Briefly, heart tissues were homogenized in ice-cold lysis buffer (60 mM KCl, 2 mM $MgCl_2$, 30 mM imidazole [pH 7.0]) supplemented with protease inhibitors (leupeptin [10 μg/mL], PMSF [0.1 mM], benzamidine [1 mM]). Homogenates were centrifuged (12,000 × *g*, 4 ℃, 15 min), and pellets were resuspended in lysis buffer containing 1% (v/v) Triton X-100 for 30 min to solubilize membranes. After three washes with lysis buffer, purified myofilaments (40 μg) were incubated in reaction buffer (32 ℃, 5 min) containing 5 mM Na_2ATP and free Ca^{2+} concentrations ranging from pCa 9.0 to pCa 4.0 (10^{-9} M to 10^{-4} M). Reactions were terminated with ice-cold 10% (w/v) trichloroacetic acid. Inorganic phosphate (Pi) release was quantified colorimetrically at 630 nm using a spectrophotometer (Ultrospec 2100, Biochrom) and calibrated against a standard curve.

2.18 Cell viability assay

To assess cell viability, we used the CCK-8 reagent according to the manufacturer's instructions (Cat. No. C266180, Aladdin Biochemical Technology, Shanghai, China). Briefly, cells were seeded in a 96-well plate at 100 μL per well, with blank wells receiving 100 μL of medium without cells, and incubated for 12 hours to allow cell attachment. Afterward, fresh media containing GSO, choline, Ang II, or both were added for treatment. The experimental groups included: Con (control, DMSO vehicle), AngII (without vehicle), AngII (with vehicle), GSO-treated AngII (AngII + GSO), and choline-treated AngII (AngII + choline). Where applicable, GSO (1 μM) or choline (1 μM) was added 2 h before Ang II (1 μM) stimulation. The working

concentrations of GSO and choline were selected based on preliminary experiments. Cells were then incubated with the appropriate treatments for 24 h (Fig S6). For the CCK-8 assay, 10 μL of CCK-8 reagent was added to each well, and after 1 hour of incubation, absorbance was measured at 450 nm using a Multiskan FC microplate reader (Thermo Fisher). Cell viability was calculated using the formula: Cell viability (%) = $[(OD_{treatment} - OD_{blank}) / (OD_{control} - OD_{blank})] \times 100\%$.

2.19 Intracellular choline levels

Intracellular choline levels were measured using a commercial Choline Assay Kit (Cat. No. ab219944, Abcam). Choline probe and AbRed indicator solutions were prepared following the manufacturer's instructions. Choline standards were serially diluted from a 50 mM stock to concentrations ranging from 30 μM to 0 μM. Cells were pretreated with GSO, stimulated with 1 μM Ang II, and collected at ~90% confluence. After washing with cold PBS, cells were lysed on ice and centrifuged at 12,000 × *g* to clarify the lysates. Choline concentrations were determined by adding 50 μL of standards or cell lysates to a 96-well plate, followed by 50 μL of choline reaction mixture. After 30 minutes of incubation in the dark, fluorescence was measured using an EnSight microplate reader at Ex/Em = 540/590 nm. A standard curve was generated, and sample concentrations were calculated based on the fluorescence values.

2.20 Cell morphology and protein expression

To validate the effects of GSO in vitro, H9C2 cells (Cat. No. iCell-r012, Saibaikang Biotechnology, Shanghai, China), HL-1 cells (Cat. No. FH1101, Fuheng Biotechnology, Shanghai, China), and AC16 cells (Cat. No. iCell-h323, Saibaikang) were used. Angiotensin II (AngII) was added to the cultures to induce cardiomyocyte hypertrophy. The cells were divided into the following groups: control (DMSO), AngII-DMSO (no vehicle), AngII (AngII + DMSO), GSO-treated AngII (AngII + GSO + DMSO), and choline-treated AngII (AngII + choline + DMSO). GSO and choline were dissolved in DMSO. Cell morphology after treatment was observed under Stellaris 5 confocal microscope (Leica Microsystems, Wetzlar, Germany). Cell surface area was measured using ImageJ software (NIH, https://imagej.nih.gov/ij). For each group, 50 cells were randomly selected for quantification.

Furthermore, to investigate the mechanisms underlying these effects, The cells from experimental groups included control, AngII, GSO-treated AngII, choline-treated AngII were collected for Western blot analysis. Briefly, following cell lysis, protein extraction, and protein concentration determination, immunoblotting was performed as described in Section 2.13 "Protein extraction and immunoblotting" using 15 μg of total protein per sample.

2.21 Statistical analysis

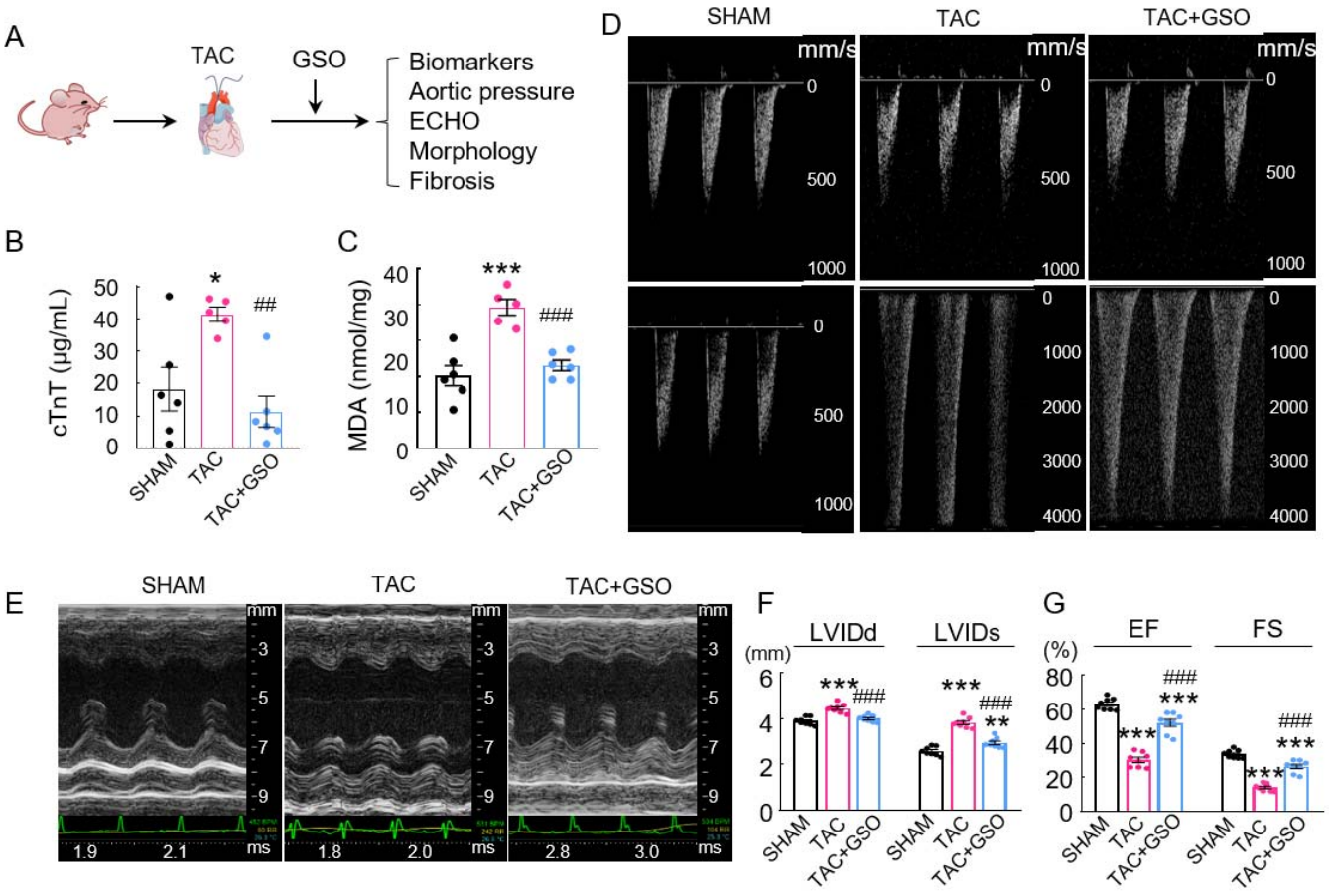
Data are presented as means ± standard error of the mean (SEM). Statistical analyses were performed using GraphPad Prism 8.0 (GraphPad Software, San Diego, CA, USA). For comparisons across multiple groups, one-way ANOVA was conducted followed by Tukey's post hoc test for all pairwise comparisons, or

by Dunnett's test when comparing multiple treatment groups against a single control group. Statistical significance was defined as $P < 0.05$.

3. Results

3.1 GSO alleviates pressure overload-induced ventricular remodeling and systolic dysfunction

To determine whether GSO protects against pressure overload-induced HF, we subjected mice to TAC and assessed cardiac injury and function 8 weeks later (Fig. 1A). GC-MS revealed multiple component classes in GSO (fatty acids, organic acids, and amino acids after derivatization), and HPLC quantified ganoderic acid subtypes B, C, D, F, and G (Table S1, Table S2, Fig. S2). Eight weeks after TAC, the HF marker cTnT and the oxidative stress marker MDA were significantly elevated; this increase was suppressed by GSO (Figs. 1B and C). Additionally, aortic systolic pressure was increased in TAC hearts (Fig. 1D). Eight weeks of pressure overload enlarged the LV internal dimensions and decreased EF and FS, which is characteristic of HFrEF. GSO effectively mitigated ventricular dilation and improved cardiac function induced by pressure overload (Figs. 1E–G). Furthermore, pressure overload induced significant cardiac hypertrophy, as evidenced by an increased heart weight-to-body weight ratio and enlarged cross-sectional heart diameter. However, these changes were inhibited by GSO (Figs. 1H and I). Additionally, pressure overload elevated the risk of cardiac fibrosis, the extent of which was significantly lower in GSO-treated hearts than in untreated hearts (Figs. 1J and K). These data establish a robust protective effect of GSO on structural remodeling and function under pressure overload.



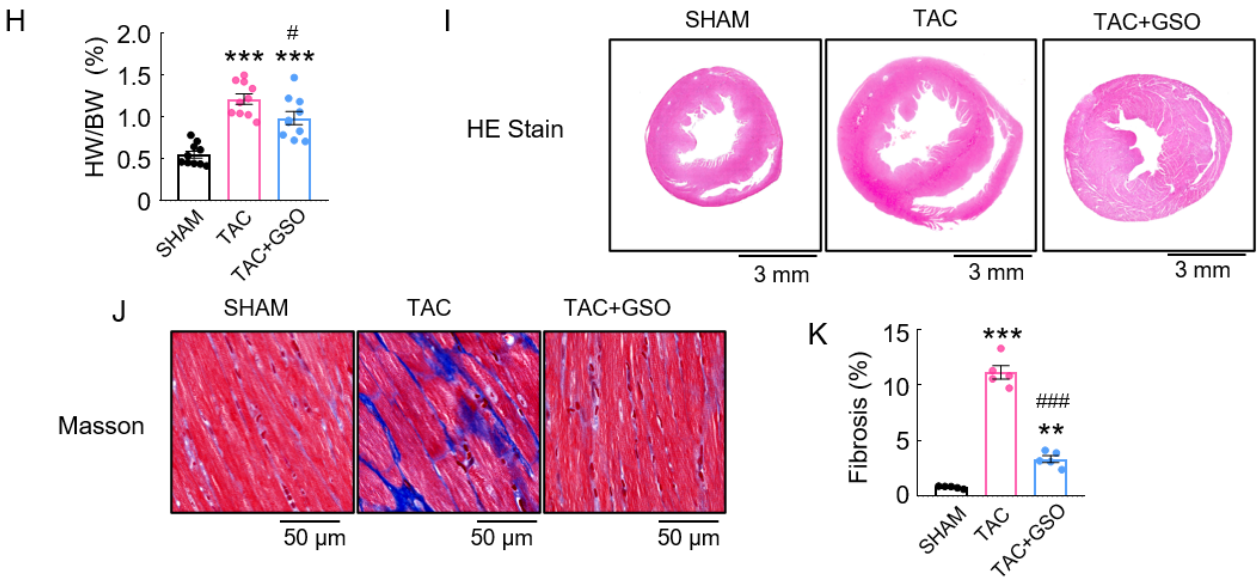


Fig. 1. **GSO alleviates pressure overload-induced ventricular remodeling and systolic dysfunction.** (A) Schematic diagram of GSO treatment in TAC mice. (B, C) Myocardial cTnT and MDA levels in the SHAM, TAC, and TAC+GSO groups (n = 5–6 mice/group). (D) Aortic pressure in the SHAM, TAC, and TAC+GSO groups (n = 8 mice/group). (E–G) M-mode echocardiography of the SHAM, TAC, and TAC+GSO groups; n = 8 mice/group. (H) Heart weight (HW) to body weight (BW) ratio. (I–K) Cross-sections stained with HE and Masson's trichrome for fibrosis assessment in left ventricular tissue (n = 5 mice/group). **P* < 0.05, ***P* < 0.01, and ****P* < 0.001 vs. SHAM. #*P* < 0.05, ##*P* < 0.01, and ###*P* < 0.001 vs. TAC. SHAM group: sham-operated mice; TAC group: mice subjected to transverse aortic constriction surgery; TAC + GSO group: TAC mice treated with GSO.

3.2 Myocardial metabolomics identifies choline depletion as a candidate target preserved by GSO

To explore how GSO confers cardioprotection, we next profiled myocardial metabolites to identify candidate biochemical mediators. Untargeted metabolomics of LV myocardium at 8 weeks post-TAC revealed broad metabolic remodeling across amino acids and derivatives (34), nucleosides/nucleotides and derivatives (20), lipids and phospholipids (10), neurotransmitters and signaling molecules (7), and other small molecules (23), energy-related and antioxidant-related compounds (5) (Fig. 2A, Fig. S3). OPLS-DA confirmed clear separation between SHAM vs. TAC, as well as between TAC vs. TAC+GSO groups (Figs. 2B and C). Among discriminating features, proline increased and choline decreased significantly with TAC (Figs. 2A and D). Importantly, GSO prevented the TAC-induced decline in myocardial choline (Figs. 2A and E). Notably, compositional analysis of GSO revealed no detectable choline (Table S1), indicating that GSO does not inherently contain choline. Instead, it appears to act through mechanisms that preserve endogenous choline levels in the myocardium. These findings establish myocardial choline depletion as a mechanism-linked alteration in pressure overload, which is reversed by GSO through preservation of endogenous myocardial choline rather than direct choline supply. Together with the compositional analysis showing that GSO itself does not contain choline, these results suggest that maintaining endogenous choline is a key pathway through which GSO exerts cardioprotection, positioning choline as a central mediator in GSO's therapeutic action.

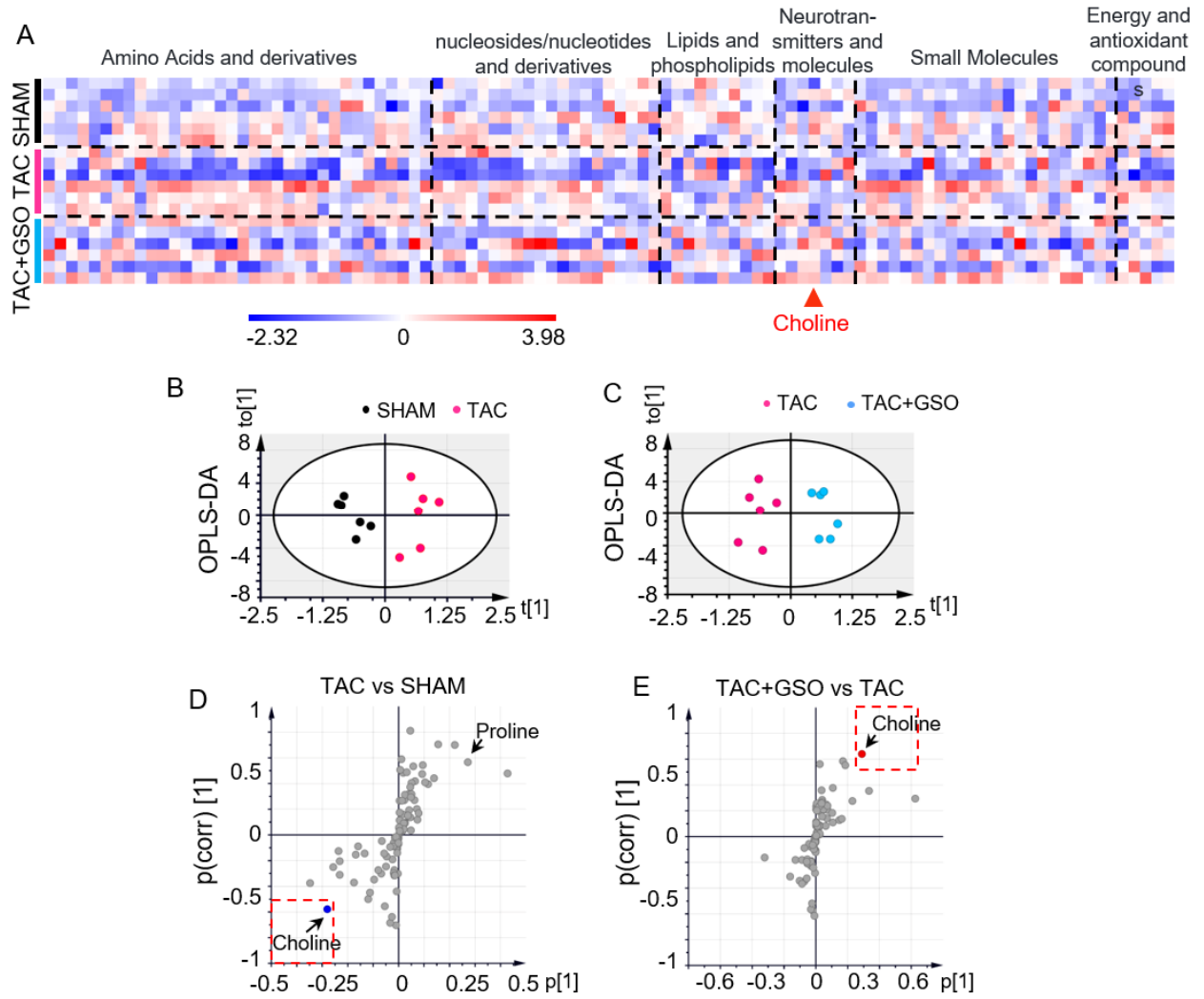


Fig. 2. Myocardial metabolomics identifies choline depletion as a candidate target preserved by GSO. (A) Heat map from metabolomics analysis for the SHAM, TAC, and TAC + GSO groups (n = 6 mice/group). (B, C) Orthogonal partial least squares discriminant analysis (OPLS-DA) comparing the SHAM vs. TAC groups and the TAC vs. TAC+GSO groups. (D, E) S-plots from OPLS-DA comparing the SHAM vs. TAC groups and the TAC vs. TAC + GSO groups.

3.3 Exogenous choline supplementation recapitulates the cardioprotective effects of GSO during the concentric-to-eccentric hypertrophy transition

We therefore hypothesized that restoring choline alone could replicate the cardioprotective effects of GSO in pressure-overloaded hearts. To test this, TAC mice were administered daily intraperitoneal injections of choline chloride. Cardiac remodeling and function were assessed at multiple stages of HF progression. Representative echocardiographic images and quantitative measurements are shown in Fig. 3A and Table S3. Blood pressure proximal to the stenosis site remained elevated at 2, 4, and 8 weeks post-TAC (Table S4), confirming persistent afterload.

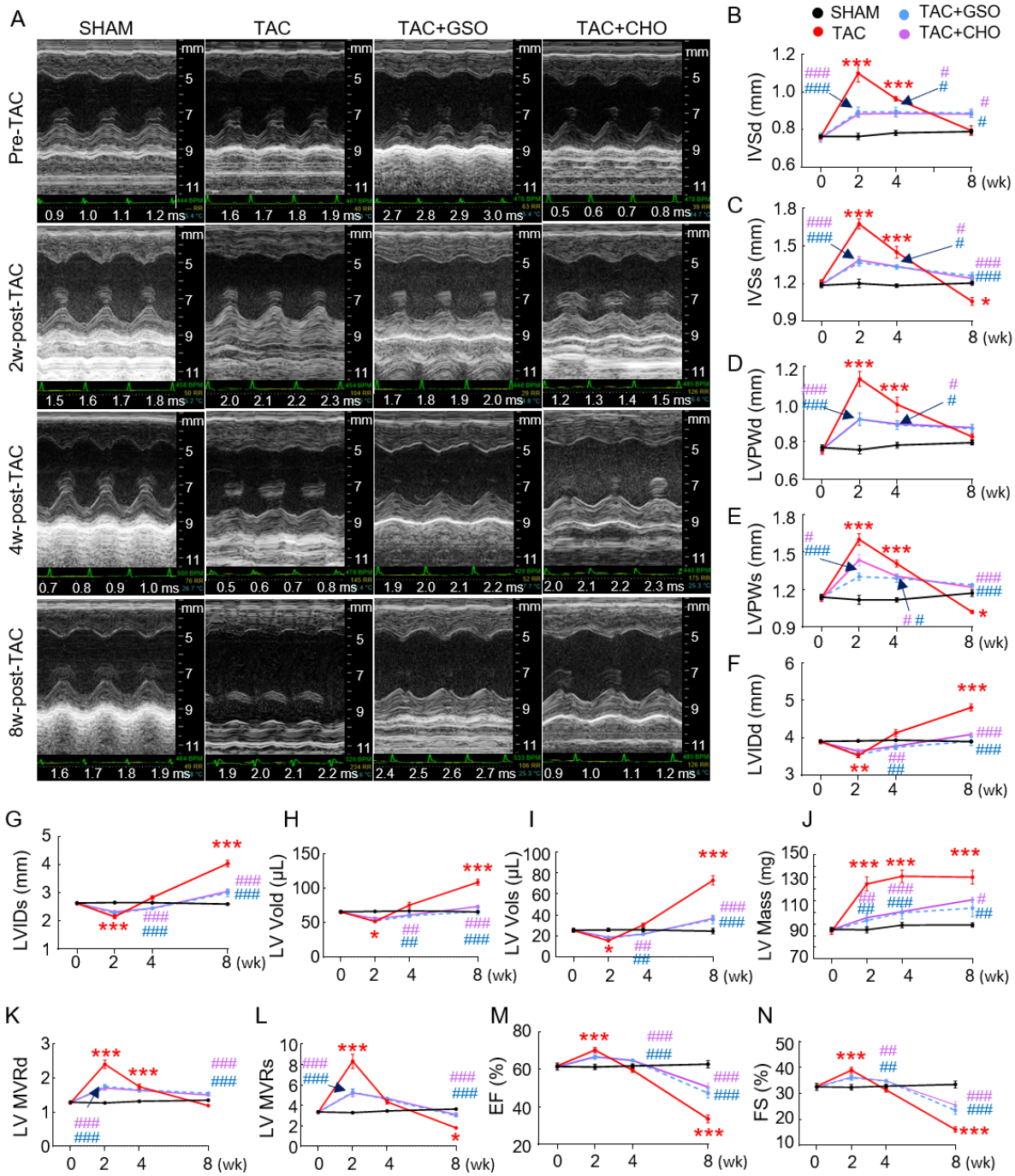


Fig. 3. Exogenous choline supplementation recapitulates the cardioprotective effects of GSO during the concentric-to-eccentric hypertrophy transition. (A) Representative M-mode echocardiography images showing the left ventricles of SHAM, TAC, TAC+GSO, and TAC+CHO mice at different time points: pre-TAC (no surgery), 2 weeks post-TAC (2w-post-TAC), 4 weeks post-TAC (4w-post-TAC), and 8 weeks post-TAC (8w-post-TAC). Echocardiographic parameters for the four groups are shown, including (B) interventricular septal thickness at end-diastole (IVSd), (C) interventricular septal thickness at end-systole (IVSs), (D) left ventricular posterior wall thickness at end-diastole (LVPWd), (E) left ventricular posterior wall thickness at end-systole (LVPWs), (F) left ventricular internal diameter at end-diastole (LVIDd), (G) left ventricular internal diameter at end-systole (LVIDs), (H) left ventricular volume at end-diastole (LV Vold), (I) left ventricular volume at end-systole (LV Vols), (J) left ventricular mass (LV Mass), (K) ratio of LV Mass to LV Vold (LV MVRd), (L) ratio of LV Mass to LV Vols (LV MVRs), (M) ejection fraction (EF), and (N) fractional shortening (FS). n = 7 mice/group. *P < 0.05, **P < 0.01, and ***P < 0.001 vs. pre-TAC. #P < 0.05, ##P < 0.01, and ###P < 0.001 vs. TAC.

Two weeks after TAC, the hearts displayed concentric hypertrophy. LV wall thickness increased during both diastole and systole (Figs. 3B–E), while the internal dimensions decreased in this phase (Figs. 3F and G).

LV systolic and diastolic volumes were reduced (Figs. 3H and I), and LV mass along with mass-to-volume ratios (LV MVRd and LV MVRs) increased significantly (Figs. 3J–L). Consequently, EF and FS were elevated (Figs. 3M and N). Choline treatment following TAC mitigated concentric remodeling. LV wall thickness was reduced (Figs. 3B–E), while chamber internal dimensions (LVIDd and LVIDs) and volumes remained unchanged (Figs. 3F–I). Increases in LV mass and LV MVR were suppressed (Figs. 3J–L). EF and FS showed no significant improvements (Figs. 3M and N), consistent with the effects of GSO treatment.

Four weeks after TAC, hearts transitioned toward eccentric hypertrophy. LV wall thickness remained elevated (Figs. 3B–E), while LVIDd and LVIDs began to enlarge (Figs. 3F and G). LV mass and LV MVRd remained high (Figs. 3J–L). However, EF and FS declined to pre-TAC baseline levels (Figs. 3M and N), indicating a transitional phase with near-baseline systolic function. Choline effectively limited ventricular expansion after 4 weeks. In comparison to untreated TAC hearts, choline significantly reduced LV wall thickness, internal dimensions, and volumes (Figs. 3B–I). It also suppressed increases in LV mass (Figs. 3J) and delayed the decline trend of EF and FS (Figs. 3M and N). These findings were comparable to those observed with GSO treatment, which also reduced cardiac remodeling and prevented the functional changes induced by pressure overload.

Eight weeks after TAC, hearts developed eccentric hypertrophy with HFrEF. This condition was characterized by LV dilation, as evidenced by increased internal dimensions and volumes (Figs. 3F–I), along with wall thinning, compared 2 and 4 weeks (Figs. 3B–E). Additionally, there was an elevation in LV mass (Fig. 3J) and a notable reduction in EF and FS to approximately 34% and 16%, respectively (Figs. 3M and N). In this HFrEF stage, choline significantly prevented wall thinning (Figs. 3B–E), attenuated cavity enlargement (Figs. 3F–I), and inhibited increases in LV mass and LV MVRd/MVRs (Figs. 3J–L), with effects consistent with those observed for GSO treatment. Consequently, choline improved EF and FS (Figs. 3M and N), demonstrating the protective effect against HFrEF induced by pressure overload.

In summary, these results confirm that exogenous choline supplementation recapitulates the cardioprotective effects of GSO in pressure-overloaded hearts. This finding indicates that choline functions as a key regulatory mediator of GSO, capable of independently eliciting similar protective effects, particularly with respect to improving cardiac remodeling and function.

3.4 Choline mitigates regional LV dysfunction and diastolic impairment induced by pressure overload

Because global echocardiographic indices may not fully capture regional dysfunction, we next evaluated myocardial motion and deformation using speckle-tracking echocardiography (Fig. 4, Fig. S4, Table S5). Radial displacement showed a significant decrease from the transitional hypertrophy stage at 4 weeks post-TAC to eccentric hypertrophy at 8 weeks (Figs. 4A and B), while longitudinal displacement began to decline as early as the concentric hypertrophy stage at 2 weeks post-TAC (Figs. 4A and C). Radial velocity decreased at 4 and 8 weeks, and longitudinal velocity decreased at 2 and 8 weeks (Figs. 4D and E). These results indicate that myocardial wall motion progressively deteriorates as the condition transitions from concentric to eccentric hypertrophy.

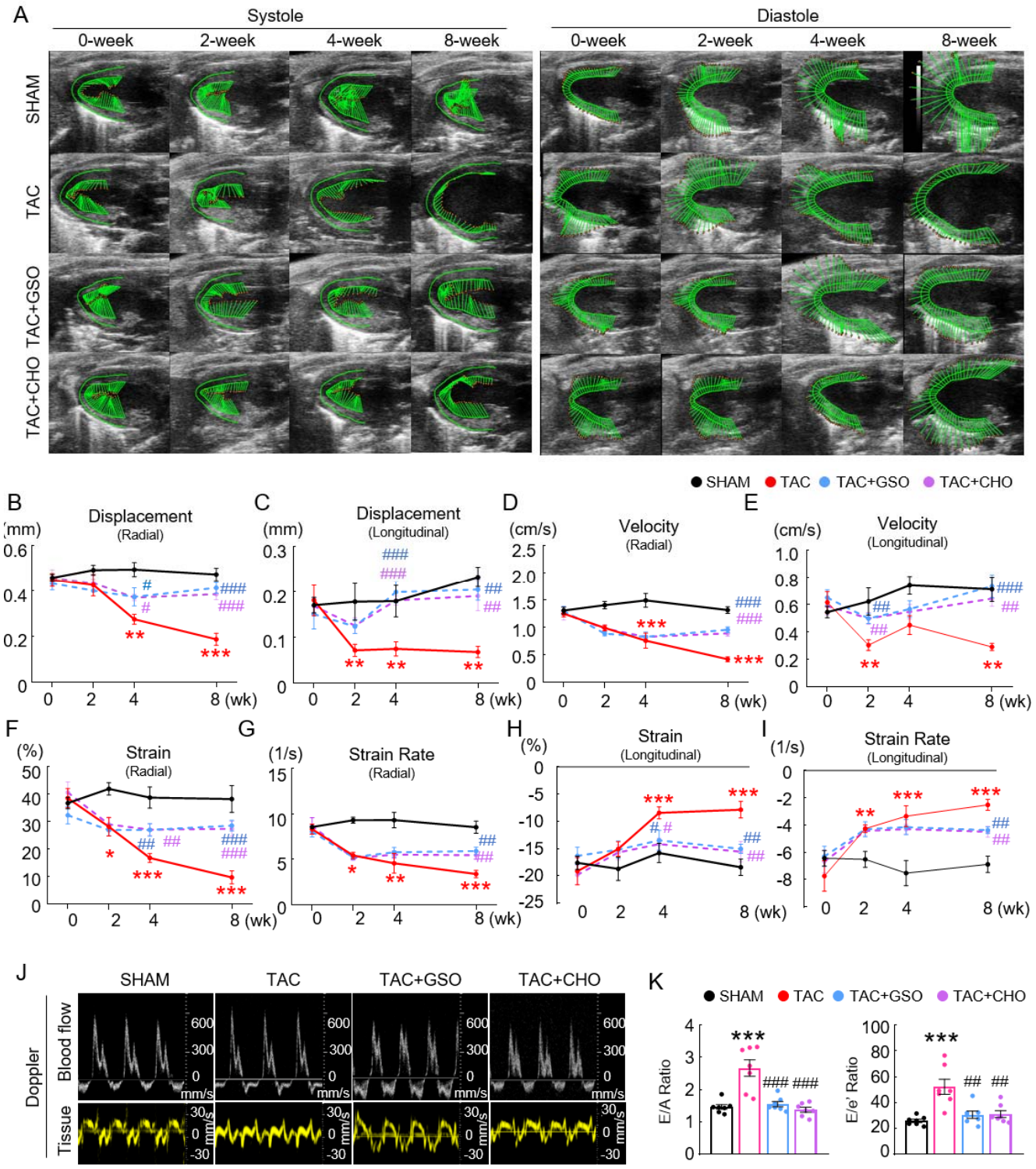


Fig. 4. Choline mitigates regional LV dysfunction and diastolic impairment under pressure overload. (A) Speckle-tracking-based strain imaging in the longitudinal plane. Serial vectors (arrows) indicate tracking of segmental myocardial deformation during left ventricular contraction from systole (left) to diastole (right). Top to bottom: SHAM, TAC, TAC+GSO, and TAC+CHO. The endocardial and epicardial borders are also traced. (B, C) Displacement (traced by vectors) of segmental myocardial deformation measured from radial and longitudinal planes. (D, E) Velocity (traced by vectors) of segmental myocardial deformation measured from radial and longitudinal planes. (F–I) Strain and strain rates measured from radial and longitudinal planes. n = 6–7 mice/group. **P* < 0.05 vs. pre-TAC; ***P* < 0.01 vs. pre-TAC; ****P* < 0.001 vs. pre-TAC. (J) Mitral inflow and tissue Doppler at 8 weeks post-TAC with or without treatments; (K) E/A and E/e′ ratios. n = 7. ****P* < 0.001 vs. SHAM. #*P* < 0.05, ##*P* < 0.01, and ###*P* < 0.001 vs. TAC.

Both LV radial strain and strain rate progressively decreased from concentric to eccentric hypertrophy (Figs. 4F and G). Longitudinal strain was significantly reduced at both 4 and 8 weeks (Figs. 4H and I), and

longitudinal strain rate showed a gradual decline post-TAC (Figs. 4H and I). Collectively, these changes reflect progressive LV deformation and dysfunction during HF development.

Choline treatment provided protection against TAC-induced LV dysfunction. At 4 and 8 weeks, choline attenuated the reduction in both radial and longitudinal displacements (Figs. 4B and C). At 8 weeks, choline also improved radial and longitudinal velocities (Figs. 4D and E). At 2 weeks, choline prevented the reduction in longitudinal velocity without affecting radial velocity (Figs. 4D and E). Importantly, the functional restoration provided by choline was progressive over time. At 4 weeks, choline improved both radial and longitudinal strain (Figs. 4F and H), and by 8 weeks, it improved strain and strain rates (Figs. 4F–I). Similarly, GSO treatment at 8 weeks reduced impairments in displacements and velocities (Figs. 4B–E) and improved strain and strain rates (Figs. 4F–I).

At 8 weeks post-TAC, the mice showed higher E/A and E/e′ ratios on echocardiography compared with the SHAM group, suggesting increased LV filling pressures (Figs. 4J and K, Table S5). Both choline and GSO attenuated these increases (Figs. 4J and K, Table S6).

These findings demonstrate that choline and GSO treatments effectively preserve regional myocardial motion and deformation, attenuating progressive LV dysfunction and diastolic impairment induced by pressure overload.

3.5 Choline reduces myocardial injury and restores electrical conduction stability in pressure-overloaded hearts

Next, we examined tissue injury and electrical activity. Histological examination revealed that 8 weeks of pressure overload increased the size of the heart, myofibrils, myocytes, and intracellular spaces, as well as the presence of inflammatory cells and fibrosis (Fig. 5A). Choline decreased the heart size, myofibril size, and the presence of inflammatory cells in TAC hearts while significantly reducing cardiac fibrosis and myocyte size (Figs. 5A–C). These effects were comparable to those elicited by GSO in TAC mice (Figs. 5A–C), where the hypertrophic phenotype was inhibited, resulting in less severe hypertrophy in hearts, myofibrils, and myocytes, as well as fewer inflammatory cells and reduced fibrosis compared to untreated TAC hearts. Furthermore, histological findings in choline-treated TAC hearts were consistent with the echocardiography results (Fig. 3), which showed that choline reduced structural changes caused by pressure overload.

Changes in electrical activity are closely associated with cardiac hypertrophy [34]. ECG analysis showed that 8-week TAC significantly prolonged P-wave duration (atrial conduction delay), QRS interval (ventricular depolarization delay), and QTc interval (ventricular repolarization abnormality) (Figs. 5D–G). Both choline and GSO treatments markedly reduced QRS interval and QTc interval (Fig. 5D–G; Table S7), indicating a restoration of normal electrical conduction.

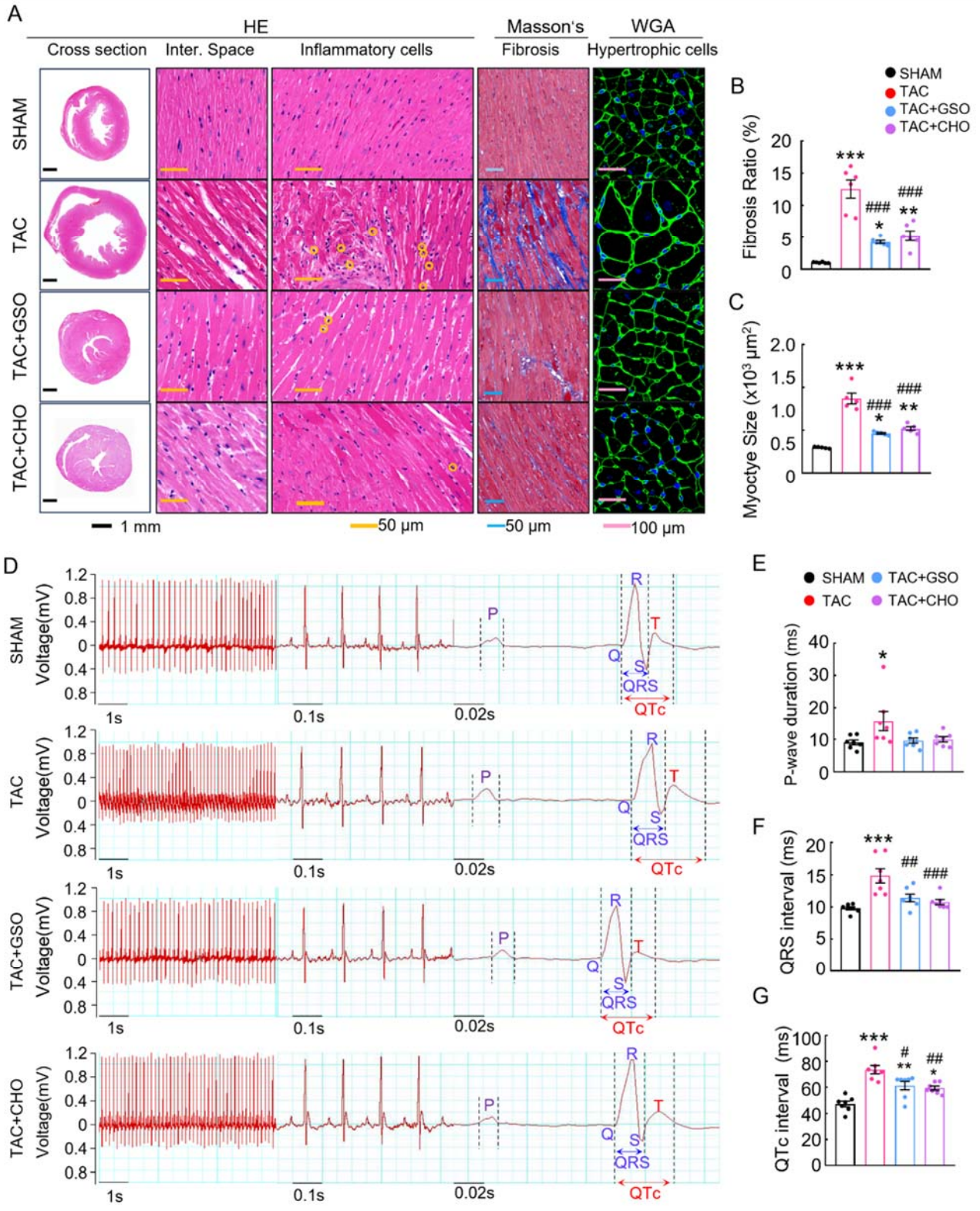


Fig. 5. Choline reduces myocardial injury and restores electrical conduction stability in pressure-overloaded hearts. (A) HE staining showing the enlarged heart (cross-section), widened interstitial space between myofibers, and inflammatory cells (lymphocytes, indicated by yellow circles) in the TAC group compared with the other three groups; Masson's trichrome staining showing fibrosis in the left ventricles; WGA staining showing hypertrophic cardiomyocytes. (B) Measurement of myocardial fibrosis ratios (n = 6 mice/group). (C) Measurement of myocyte size (n = 5 mice/group). (D) ECG recordings from each experimental group at different time scales, with a close-up view of a single beat for each group. Measurements of (E) P-wave duration, (F) QRS complex interval, and (G) heart rate-corrected QT interval (QTc) for the SHAM, TAC, TAC+GSO, and TAC+CHO groups (n = 7 mice/group). *P < 0.05, **P < 0.01, and ***P < 0.001 vs. SHAM. #P < 0.05, ##P < 0.01, and ###P < 0.001 vs. TAC.

RNA-seq analysis (accession No. GSE 278386) identified arrhythmia-associated DEGs in "TAC vs. SHAM", "GSO+TAC vs. TAC", and "CHO+TAC vs. TAC" groups (Table 1). TAC downregulated *Kcna5, Abcc9, Scn10a,* and *Cacna1e* expression at 8 weeks; this was reversed by both GSO and choline. Additionally, TAC upregulated *Kcng2, Kcnj4, Trpm2*, *Cacnb1,* and *Cacnb3*, which were suppressed by GSO but not significantly downregulated by choline. These results suggest that choline, like GSO, modulates specific arrhythmia-related genes to protect electrical activity in pressure-overloaded hearts.

Table 1. Fold changes and P-values of ion channel differentially expressed genes (DEGs) in each group.

Gene ID	Protein Name	TAC vs. SHAM		TAC+GSO vs. TAC		TAC+CHO vs. TAC	
		log_2FC	-log(P)	log_2FC	-log(P)	log_2FC	-log(P)
KCNA5	Potassium voltage-gated channel subfamily A member 5 (Kv1.5)	-0.69	5.28	0.51	3.13	0.82	0.15
ABCC9	ATP-binding cassette sub-family C member 9 (ABCC9, or SUR2)	-0.83	9.11	0.30	1.22	2.02	0.01
SCN10A	Sodium channel voltage-gated type 10 alpha subunit (Nav1.8)	-1.15	3.75	0.68	1.42	0.60	0.25
CACNA1E	Calcium voltage-gated channel subunit alpha1E (Cav2.3)	-0.91	1.40	0.14	0.08	1.41	0.04
KCNG2	Potassium channel subfamily G member 2 (Kv6.2)	0.86	3.10	-0.10	0.19	1.39	0.04
KCNJ4	Potassium channel, inwardly rectifying subfamily J member 4 (Kir 2.3)	1.32	3.06	-0.84	1.43	1.12	0.08
TRPM2	Transient receptor potential cation channel subfamily M member 2 (TRPM2)	1.10	2.54	-0.42	0.60	2.57	0.00
CACNB1	Calcium voltage-gated channel subunit beta-1 (Cavβ1)	0.99	5.91	-0.28	0.89	1.45	0.04
CACNB3	Calcium voltage-gated channel subunit beta-3 (Cavβ3)	1.08	7.12	-0.17	0.37	2.69	0.00

Note: The comparison groups include TAC vs. SHAM, TAC+GSO vs. TAC, and TAC+CHO vs. TAC. n = 5 mice/group. "P" represents the adjusted p-value.

3.6 Choline and GSO converge on hypertrophy signaling and suppress the RAF/MEK/ERK cascade

To elucidate the underlying mechanisms, we next examined hypertrophy-related signaling networks and identified key regulatory nodes. RNA-seq-based IPA revealed the expression of 30,740 genes in hearts 8 weeks post-TAC. Based on a FC threshold of 1.5 and P-value < 0.05, 1,849 genes were upregulated and 1,295 genes downregulated following TAC. These DEGs were predominantly enriched in the "Cardiac Hypertrophy Signaling (enhanced)" pathway (-Log10(P-value) = 6.161; Fig. 6, Fig. S5; Table S8). The "Cardiac Hypertrophy Signaling (enhanced)" pathway, as defined by IPA, mediates cardiac hypertrophy by promoting abnormal myocardial enlargement due to myocyte hypertrophy. Initially, this is an adaptive response aimed at normalizing wall tension and maintaining cardiac output; however, sustained pressure overload leads to pathological progression and HF.

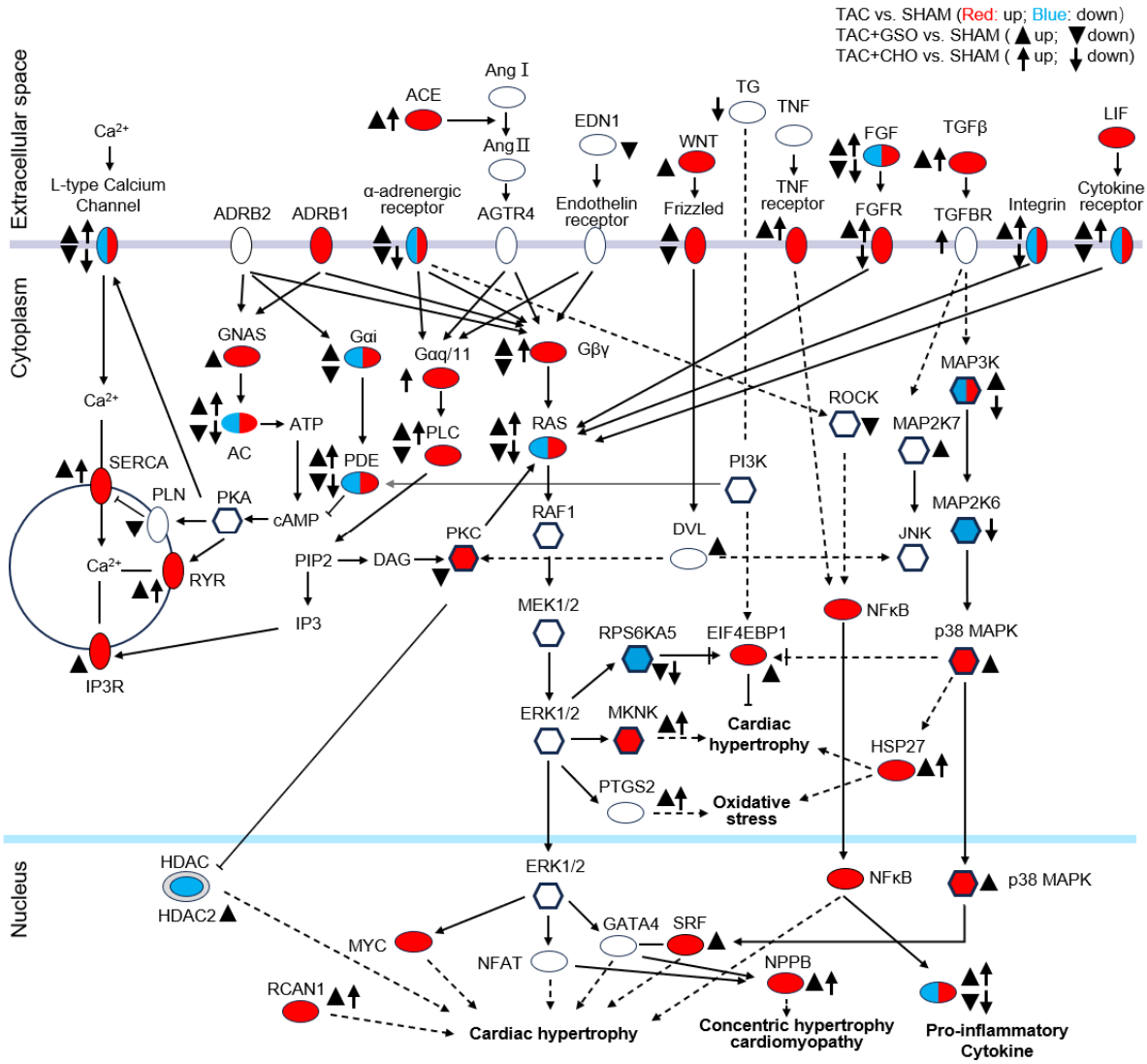


Fig. 6. Choline and GSO converge on hypertrophy signaling in pressure-overload hearts. Ingenuity Pathway Analysis (IPA) identified intracellular pathways targeted by GSO or choline, using differentially expressed genes (DEGs) from three pairwise comparisons: "TAC vs. SHAM", "TAC+GSO vs. SHAM", and "TAC+CHO vs. SHAM". The full gene names corresponding to each gene ID are listed in Table S7. Hexagons: protein kinases in the signaling pathways; solid arrows: direct interactions; dashed arrows: indirect interactions; vertical bars: inhibition or ubiquitination; arrows with vertical bars: inhibition and action on the target.

In hearts 8 weeks post-TAC, receptor-dependent signaling pathways activated by pressure overload included β1- and α-adrenergic receptors via $G_{\beta\gamma}$/RAS signaling, α-adrenergic receptors through Gαq/11/PKC/RAS signaling, and FGFR, integrins, and cytokine receptors via RAS signaling. Additionally, these pathways could trigger the mitogen-activated protein kinase (MAPK) cascade (RAF/MEK/ERK), leading to cardiac hypertrophy and oxidative stress through PTGS2. Furthermore, α-adrenergic or TNF receptors via NFκB signaling activate pro-inflammatory cytokines, while the activation of intracellular P38 MAPK/HSP27 by pressure overload can induce cardiac hypertrophy or oxidative stress. Notably, nuclear P38 MAPK directly influences hypertrophic transcription factors.

When compared to the SHAM group, the TAC+GSO group exhibited 3,460 DEGs, with 1,801 upregulated and 1,659 downregulated genes. In contrast, the TAC+CHO group showed 1,758 DEGs, including 1,104 upregulated and 654 downregulated genes. To understand the involvement of signaling

pathways related to cardiac hypertrophy, we compared DEGs between the "TAC+GSO vs. SHAM" and "TAC+CHO vs. SHAM" groups, focusing on genes associated with the enhanced cardiac hypertrophy signaling pathway (Fig. 6, Table S8). For genes that modulate cardiac hypertrophy, GSO and choline restored the expression of four key families: ADRB1, LIF, NF-κB, and MYC. However, two gene families (Gαq/11 and MAP2K6) were specifically restored by GSO, while choline uniquely restored nine other families, including WNT, Frizzled, P38 MAPK, SRF, PKC, EIF4EBP1, GNAS, IP3R, and HDAC2. Interestingly, 23 gene families, such as ACE, α-adrenergic receptor, RAS, and others, were not restored by either treatment. Furthermore, eight gene families (EDN1, TG, TGFBR, ROCK, DVL, MAP2K7, PTGS2, and PLN) did not change in the untreated TAC hearts but exhibited significant alterations in hearts treated with GSO or choline. Notably, at the final signaling nodes involved in hypertrophy, oxidative stress, and concentric hypertrophic cardiomyopathy, both GSO and choline regulated MYC and NF-κB in pressure-overloaded hearts. In summary, both GSO and choline converge on MAPK signaling as a major pathway mediating their beneficial effects in pressure-overloaded hearts.

These findings prompted us to further validate the role of MAPK signaling in mediating the observed effects. To validate IPA predictions, we focused on the MAPK pathway (RAS→RAF1→MEK1/2→ERK1/2; Fig. 7A). Pressure overload significantly elevated the phosphorylation of RAF1, MEK1/2, and ERK1/2 in TAC hearts ($P < 0.05$ vs. SHAM; Figs. 7B–E). Both choline and GSO treatments suppressed the phosphorylation of these kinases ($P < 0.05$ vs. TAC), confirming that they attenuate the RAF/MEK/ERK hypertrophic cascade in the setting of pressure overload–induced choline deficiency.

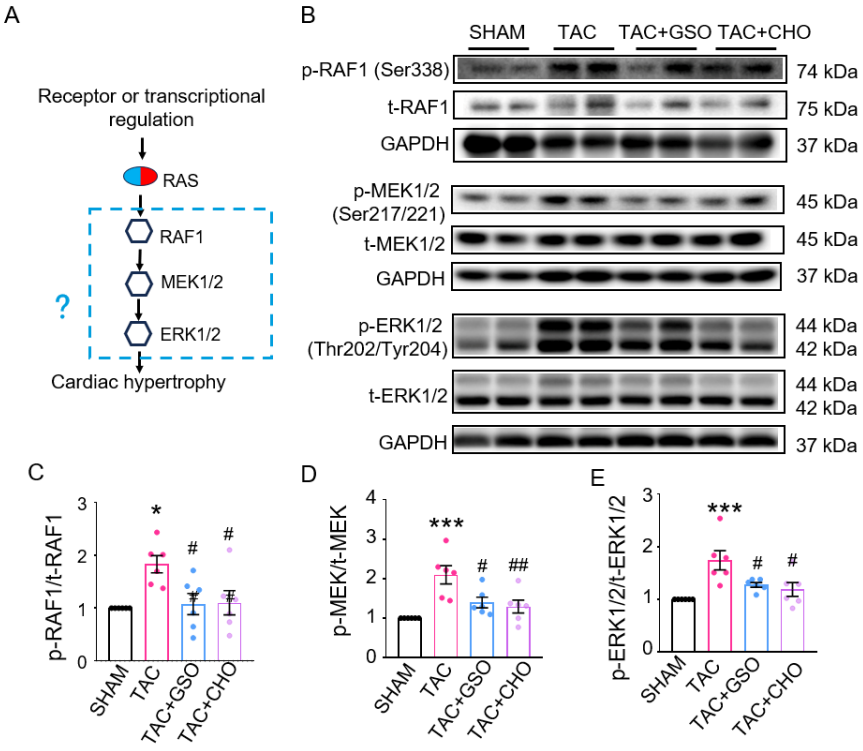


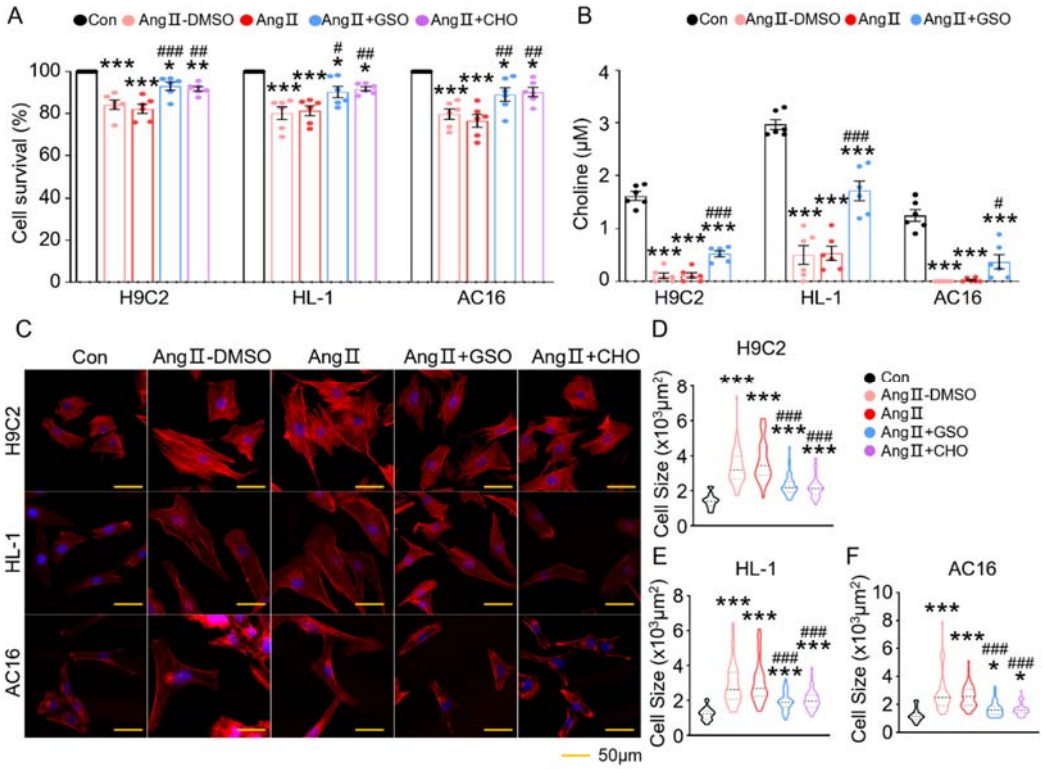
Fig. 7. Choline suppress RAF/MEK/ERK cascade in pressure-overloaded hearts. (A) Schematic diagram of the RAF/MEK/ERK signaling pathway activated in response to pressure overload, as shown in the Ingenuity Pathway Analysis (IPA) in Fig. 6. Western blot analysis of phosphorylated and total RAF1 (B, C), phosphorylated and total MEK1/2 (B, D), and phosphorylated and total ERK1/2 (B, E) (n = 6 mice/group); n = 6 mice/group. $^{**}P < 0.01$ and $^{***}P < 0.001$ vs. SHAM. $^{\#}P < 0.05$ and $^{\#\#}P < 0.01$ vs. TAC.

3.7 In vitro model supports that GSO targeted hypertrophic phenotypes

To further validate our in vivo findings, we next turned to in vitro models to investigate the cellular mechanisms underlying GSO's effects on hypertrophic signaling. The viability of the cells and intracellular choline levels were reduced in the H9C2, HL-1, and AC16 cells stimulated with AngII. However, both cell viability and intracellular choline levels were significantly restored by GSO treatment (Fig. 8A and B). These findings are consistent with our in vivo experiments, which showed that GSO prevents the reduction of choline levels, and this preservation was associated with the inhibition of cardiac hypertrophy. Furthermore, in the in vitro experiments, we observed that AngII-induced enlargement of H9C2, HL-1, and AC16 cells was significantly suppressed by supplementation with GSO or choline (Figs. 8C–F), indicating that both GSO and choline can inhibit the hypertrophic phenotype. These results further support the hypothesis that GSO targets the hypertrophy observed in in vivo TAC mouse models, while also highlighting the crucial role of choline in modulating this phenotype.

In vitro, H9C2 cells subjected to hypertrophic stimulation exhibited increased phosphorylation levels of RAF1, MEK1/2, and ERK1/2. These elevated phosphorylation levels were significantly reduced by GSO or choline treatment (Figs. 8G–J). These results are consistent with those observed in the in vivo models, where hypertrophic cardiomyocytes in failing TAC hearts also showed altered RAF-MEK-ERK signaling. This further confirms that GSO targets the RAF-MEK-ERK signaling pathway in both in vitro and in vivo settings.

In summary, these results further support choline as a key regulatory factor, particularly at the signaling pathway level. We demonstrate that both GSO and choline inhibit the RAF/MEK/ERK cascade, a central pathway in cardiac hypertrophy signaling. This convergence highlights choline's role as a mediator of the cardioprotective effects induced by GSO.



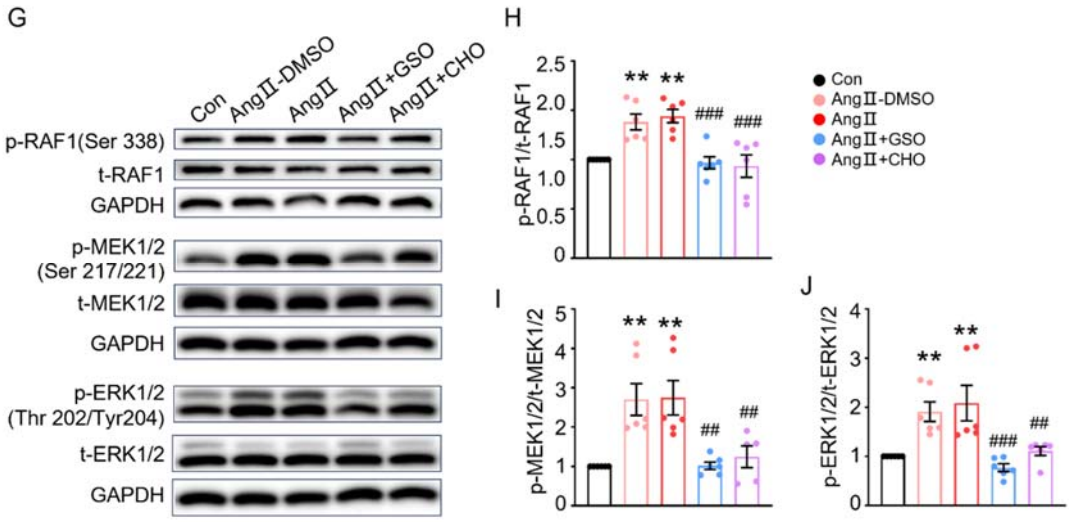


Fig. 8 GSO ameliorates hypertrophic phenotypes in cardiomyocyte cell lines in vitro. (A) Under AngII-induced hypertrophic conditions, the viability of H9C2, HL-1, and AC16 cells was significantly decreased, and this decrease was significantly reversed by treatment with GSO or choline.(B) Intracellular choline levels in H9C2, HL-1, and AC16 cells were significantly reduced under hypertrophic conditions, and this reduction was significantly reversed by treatment with GSO or choline. (C–F) The cellular sizes of H9C2, HL-1, and AC16 cells treated with AngII were significantly increased, and this increase was significantly reduced by supplementation with GSO or choline. (G–J) Phosphorylation levels of RAF1, MEK1/2, and ERK1/2 in H9C2 cells were elevated under hypertrophic conditions and were significantly reduced by GSO or choline treatment. **P* < 0.05, ***P* < 0.01, and ****P* < 0.001 vs. CON; #*P* < 0.05, ##*P* < 0.01, and ###*P* < 0.001 vs. AngII; **P* < 0.001 vs. AngII. n = 6. Con (control group, DMSO vehicle), AngII-DMSO (treated with AngII without vehicle), AngII (AngII + vehicle), GSO-treated AngII (AngII + GSO), and choline-treated AngII (AngII + choline).

3.8 Choline restores myocardial ATP supply, calcium handling, and sarcomere mechanics

As energy supply and calcium handling are crucial for cardiac contractile function and are downstream of hypertrophic signals, we next evaluated ATP production and myofilament function. At eight weeks post-TAC, ATP levels in pressure-overloaded hearts were significantly reduced compared to SHAM mice. However, both choline and GSO treatments restored ATP production to normal levels in the pressure-overloaded hearts (Fig. 9A).

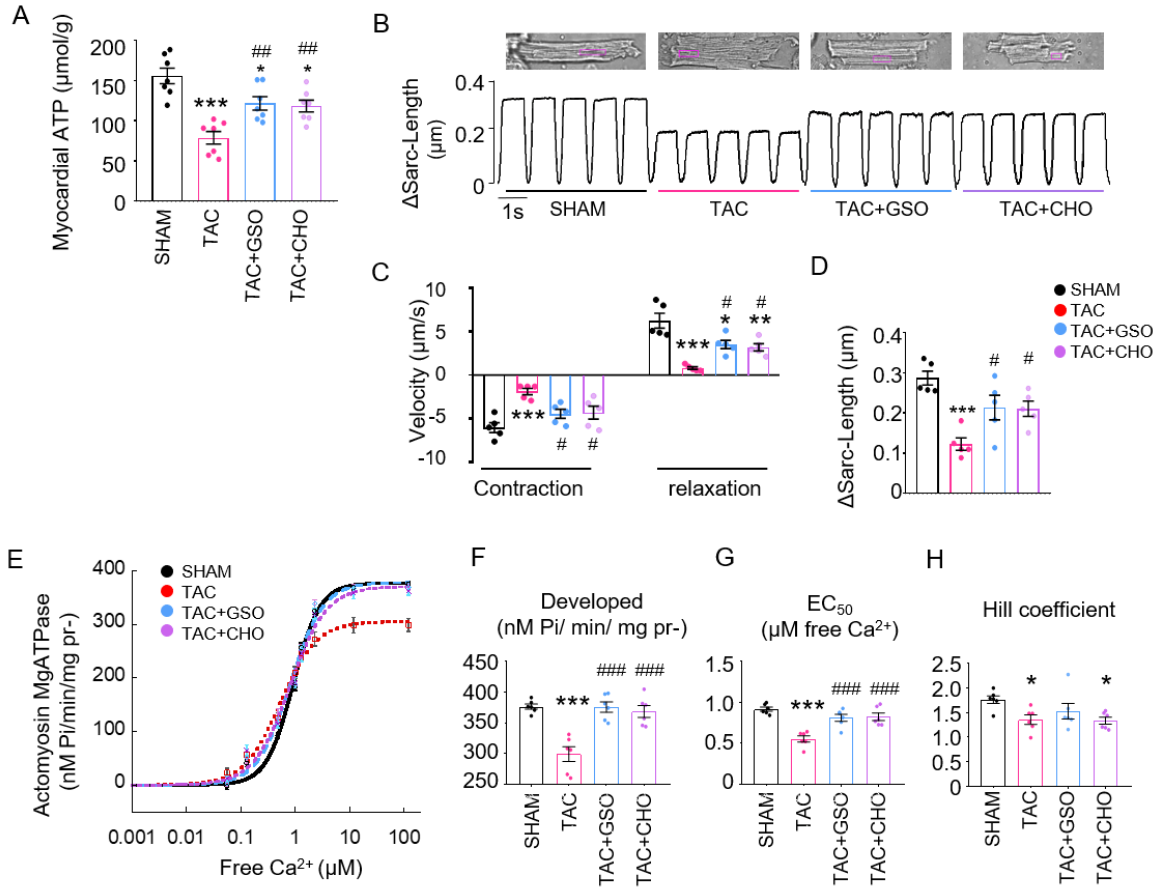


Fig. 9. Choline restores myocardial ATP supply, calcium handling, and sarcomere mechanics. (A) GSO and choline restore myocardial ATP generation under pressure overload conditions (n = 7 mice/group). (B) GSO and choline normalize changes in sarcomere length during contraction and relaxation (n = 5 mice/group). (C) Velocities of myocyte shortening (contraction; negative) and lengthening (relaxation; positive). (D) Sarcomere length during the contraction–relaxation cycle. (E–H) GSO and choline ameliorate the abnormalities in actomyosin MgATPase activity and Ca^{2+} sensitivity of myofilaments under pressure overload (n = 6 mice/group). **P* < 0.05, ***P* < 0.01, and ****P* < 0.001 vs. SHAM. #*P* < 0.05, ##*P* < 0.01, and ###*P* < 0.001 vs. TAC.

In addition, IPA analysis revealed substantial alterations in calcium signaling pathways in hearts subjected to 8 weeks of pressure overload (Fig. 6). Specifically, these changes included: (1) alterations in L-type calcium channels and SERCA; (2) activation of ADRB1, with subsequent modulation of GNAS/AC or $G_{\alpha i}$/PDE pathways, and increased expression of RYRs (involving ATP conversion to cAMP); and (3) α-adrenergic activation of $G_{\alpha q/11}$/PLC with elevated IP3R expression. Compared to untreated TAC hearts, both GSO and choline normalized ADRB1 expression, with choline alone restoring the expression of IP3R, GNAS, and $G_{\alpha i}$ (Fig. 6). These findings suggest that the cardioprotective effects of GSO and choline in pressure-overloaded hearts may be linked to improved calcium handling.

We further assessed the role of GSO and choline in regulating calcium-dependent myocyte contractility in pressure-overloaded hearts. Pressure overload significantly impaired myocyte shortening (negative) and lengthening (positive) velocities, as well as sarcomere length during the contraction–relaxation cycle (Figs. 9B–D). However, choline effectively restored both myocyte velocities and sarcomere length (Figs. 9B–D), with similar results observed following GSO treatment (Figs. 9B–D).

Given the metabolic abnormalities and reduced ATP availability in pressure-overloaded myocardium, we also investigated changes in actomyosin MgATPase activity, an enzyme complex responsible for sarcomere

movement and force generation. In TAC hearts, actomyosin MgATPase activity was significantly suppressed after 8 weeks, which correlated with increased calcium sensitivity and a reduced Hill coefficient, indicating altered myofilament contractility in response to calcium (Figs. 9E–H). Choline treatment restored actomyosin MgATPase activity, partially restored calcium sensitivity but not the Hill coefficient. GSO treatment also produced similar effects in pressure-overloaded hearts (Figs. 9E–H).

These findings demonstrate that both GSO and choline play pivotal roles in restoring energy and calcium handling in pressure-overloaded hearts. By improving ATP supply and enhancing calcium signaling, both treatments contribute to the normalization of myocardial function and the maintenance of sarcomere mechanics, highlighting the therapeutic potential of GSO and choline in mitigating the functional impairments caused by pressure overload.

4. Discussion

This study identifies preservation of myocardial choline as a central mediator within the multi-component cardioprotective network elicited by GSO against pressure overload-induced HFrEF. We base this conclusion on three converging lines of evidence. First, under chronic pressure overload, untargeted metabolomics revealed that myocardial choline is markedly depleted, and GSO selectively restores this deficit. Second, low-dose choline supplementation alone largely recapitulates the structural, functional, and molecular benefits of GSO, including attenuation of fibrosis and inflammation, preservation of both systolic and diastolic myocardial deformation, enhancement of electrical stability, and prevention of bioenergetic failure. Third, integration of transcriptomic, biochemical, and functional analyses shows that both GSO and choline converge on suppression of pro-hypertrophic RAF/MEK/ERK signaling, normalization of calcium handling, and restoration of actomyosin ATPase-driven contractility, even though compositional analysis confirms that GSO itself does not contain choline. Together, these data indicate that GSO acts by preserving endogenous myocardial choline levels rather than providing choline directly. These converging findings provide a clear mechanistic rationale for considering choline a key regulatory mediator of the cardioprotective actions of GSO and unveil a previously unidentified metabolic–signaling axis in the progression of pressure overload-induced HF.

4.1 GSO and choline preserve cardiac structure and function across hypertrophic transition

We demonstrated that GSO confers sustained protection through all major phases of pressure overload–induced HF progression (2, 4, and 8 weeks post-TAC), limiting wall thickening in concentric hypertrophy, constraining chamber dilation in the transitional phase, and mitigating wall thinning and EF decline during established eccentric hypertrophy. Previous studies have consistently demonstrated that increased LV mass (LVM) is an independent predictor of cardiovascular events, cardiovascular mortality, and all-cause mortality [35]. Consequently, reversing hypertrophy has been a long-standing therapeutic aim.

Traditionally, treatment of hypertrophy has relied on pharmacological targeting of pressure overload, particularly through inhibitors of the renin-angiotensin-aldosterone system (RAAS) [36]. However, in our study of HFrEF hearts, we observed that the expression of the Ang II-dependent AGTR4 gene did not exhibit

significant changes. This suggests that in the advanced stages of HF, the RAAS pathway may no longer play a dominant regulatory role in hypertrophic signaling. On this basis, GSO presents itself as a novel, RAAS-independent therapeutic approach. In patients with hypertensive heart disease and end-stage HF, GSO may not only serve as a valuable adjunct to existing therapy but could also represent an effective alternative strategy for the management of hypertrophy.

A key mechanistic advancement is the discovery that GSO restores physiological myocardial choline levels lost under chronic pressure overload. Choline is essential for membrane phospholipid synthesis, methylation reactions, and acetylcholine production. Animal studies have demonstrated that choline deficiency impairs cardiac development and function [24, 37]. Although excessive dietary choline can be converted by the gut microbiota to TMAO, which has been associated with adverse cardiovascular outcomes [26], our protocol administered low-dose intraperitoneal choline, thereby bypassing the microbiota-dependent pathway and approximating the physiological repletion achieved with GSO [25, 38, 39]. This dose was sufficient to largely replicate the benefits of GSO across major structural and functional domains without the potential risk of TMAO-mediated harm. Importantly, our results formalize an experimentally tractable "metabolite rescue" strategy that links a natural product's complex bioactivity to a specific metabolic deficiency in target tissue, and, together with compositional data showing that GSO does not inherently contain choline, indicate that GSO primarily acts by maintaining endogenous myocardial choline levels rather than serving as an exogenous choline source. In this context, we consider choline a key regulatory mediator through which GSO exerts a substantial proportion of its cardioprotective effects under pressure overload.

4.2 Choline-dependent preservation of contractile performance and electrical stability in eccentric hypertrophy

In hearts with HFrEF, calcium handling and ATP production are dysfunctional; both are integral to cardiac contractile function, as the contraction is calcium-dependent and requires ATP as an energy source. Therefore, we investigated how GSO and choline may prevent HFrEF by restoring cardiac contractile function through these mechanisms.

Myocardial contraction is initiated when a low calcium concentration enters cardiomyocytes through L-type calcium channels, triggering the mass release of calcium from the sarcoplasmic reticulum via RYRs. The resulting increase in intracellular calcium promotes its binding to the troponin complex on actin filaments and, with ATP as the energy source, generates the force required for contraction [40, 41]. Cardiomyocyte relaxation occurs once appropriate extracellular and intracellular ion concentrations are restored. Pressure overload induces an imbalance in calcium handling [42]. We observed that pressure overload altered L-type calcium channel expression and upregulated SERCA, RYR, and IP3R expression. In contrast, GSO and choline specifically modulated the expression of genes associated with calcium signaling in pressure-overloaded hearts. Furthermore, calcium-dependent changes in sarcomere length were consistently decreased in the hearts of mice with pressure overload-induced HFrEF. However, GSO and choline restored

the calcium-dependent sarcomere lengths. These effects are also reflected in the improved EF and FS, as well as the enhanced cardiac motion in hearts treated with GSO or choline.

Various pathological conditions can induce metabolic disturbances in the heart, leading to inadequate ATP production and compromised myocardial contractile function. Our findings demonstrate that ATP production is diminished in pressure-overloaded myocardium with reduced myocardial choline levels. However, GSO and choline supplementation effectively restored ATP production, highlighting the role of choline in supporting the protective effects of GSO. This suggests that choline supplementation may directly improve myocardial metabolic function in the context of pressure overload. Similar to other forms of cardiac injury, such as ischemia-reperfusion injury [30, 33, 43], the activity of actomyosin MgATPase is impaired in pressure-overloaded hearts. In this study, GSO restored actomyosin MgATPase activity, thereby helping to preserve cardiac contractile function by re-establishing metabolic processes and enhancing ATP utilization. These effects were also observed in choline-supplemented, pressure-overloaded hearts, further confirming that choline plays a critical role in GSO-mediated cardiac protection.

The normal pumping function of the heart results from the coordinated interaction of multiple physiological processes. In addition to metabolic activity, myocardial cell function, and intracellular signaling regulation, electrical activity is pivotal. TAC hearts exhibited prolonged conduction and repolarization intervals, consistent with arrhythmogenic remodeling. Choline and GSO both restored expression of ion channel genes such as Kcna5 and Abcc9, which encode Kv1.5 and the SUR2 subunit of KATP channels, respectively; these proteins play key roles in atrial repolarization and metabolic stress adaptation [44, 45]. These coordinated molecular corrections paralleled normalization of ECG parameters [46-50], suggesting that the choline axis not only supports structural and mechanical function but also restrains the electrical substrate for arrhythmias in pressure-overloaded hearts.

4.3 Suppression of pathological hypertrophy signaling as a unifying mechanism

The cardioprotective effects of *G. lucidum* (Reishi) involve modulating multiple signaling pathways. Liang et al. reported that treatment with *G. lucidum* polysaccharides reduced the phosphorylation of ERK, p38, JNK, and AKT in lipopolysaccharide-induced human aortic smooth muscle cells. This was associated with inhibiting NF-κB p65 translocation and reducing IL-1β expression [51]. In Ang II-treated cardiomyocytes and TAC mouse models, *G. lucidum* polysaccharides alleviate myocardial hypertrophy and cardiac enlargement by upregulating PPARγ and PGC-1α expression [52]. In doxorubicin-induced cardiotoxicity models, *G. lucidum* polysaccharides inhibit cardiomyocyte apoptosis by downregulating BAX expression and increasing BCL-2 expression [53]. In bovine aortic endothelial cells, *G. lucidum* triterpenoids reduce SMAD2/3, ERK1/2, AKT, GSK-3β, and Snail phosphorylation in response to homocysteine [54]. In rat models of TMAO-induced heart dysfunction, *G. lucidum* spore extract modulates the expression of proteins involved in energy metabolism (e.g., MTND2 and FASN) and inflammation (e.g., S100A8 and S100A9) [18].

In the present study, we delineated the signaling pathways activated in pressure-overload-induced HFrEF, including those involved in regulating L-type calcium channels, β-adrenergic receptors, α-adrenergic receptors, ACE, Frizzled receptors, cytokine receptors, integrins, FGFRs, TGF-β, and TNF receptors. These pathways are consistent with those previously identified as associated with myocardial hypertrophy. Notably, the effects of GSO in pressure-overloaded hearts overlap with those seen in choline-supplemented models. Both GSO and choline help to modulate critical pathways, such as TGF-β and TNF signaling, that are central to the regulation of hypertrophy and fibrosis in HF. For example, alterations in the density of L-type calcium currents are observed as myocardial hypertrophy develops and progresses to HF [55], while sustained activation of β1-adrenergic receptors promotes myocardial hypertrophy, ultimately leading to HF [56].

Moreover, choline itself plays a central role in modulating these hypertrophy-related pathways. As shown in our study, choline supplementation alleviates pressure-overload-induced hypertrophy by by improving myocardial bioenergetic status and calcium handling. These mechanisms are closely intertwined with the cardioprotective actions of GSO, suggesting that choline, as a key metabolic mediator, makes a substantial contribution to the suppression of pathological hypertrophic signaling. Together, these results highlight the unique role of choline in supporting the beneficial effects of GSO and emphasize its function as a pivotal regulator in the context of pressure-overload-induced HF. This integrated analysis provides a more detailed understanding of the specific signaling molecules targeted by GSO and choline in pressure-overloaded hearts, underscoring their capacity to suppress pathological hypertrophic signaling and preserve cardiac structure and function.

4.4 Limitations

This study has several limitations. First, while we identify modulation associated with choline affecting prohypertrophic RAF/MEK/ERK signaling, calcium handling, and contractility linked to actomyosin ATPase activity, the causal hierarchy remains to be established. Validating these mechanisms will require targeted loss- and gain-of-function interventions and multi-omics flux studies. Second, although our data support preservation of myocardial choline as a key mechanism of GSO-mediated cardioprotection, the upstream regulatory mechanism by which GSO maintains choline homeostasis remains incompletely defined. In particular, we did not determine whether GSO acts primarily on choline transport, biosynthesis, utilization, or turnover, nor did we identify the specific constituent(s) within this multi-component preparation that are responsible for modulating choline metabolism. Future studies will need to isolate and characterize individual GSO components and combine metabolomics, isotope-tracer flux analyses, and targeted molecular interventions to dissect how GSO regulates myocardial choline at the mechanistic level.

Third, we did not perform comprehensive chemoprofiling of other bioactive constituents derived from GSO or downstream metabolites that may exert additive or synergistic cardioprotective effects; untargeted metabolomics and isotope tracer flux analyses are needed to map these contributions. Finally, all experiments were conducted in a murine pressure overload HF model, which cannot fully recapitulate the

genetic, metabolic, and clinical heterogeneity of human HF. Translation will require validation in platforms relevant to humans (for example, cardiomyocytes derived from induced pluripotent stem cells, cardiac organoids, large animal models) and ultimately rigorously designed clinical trials.

5. Conclusion

This study demonstrates that GSO mitigates pressure overload induced HFrEF progression, delaying the shift from concentric to eccentric remodeling, reducing fibrosis and inflammation, preserving systolic and diastolic function, and enhancing electrical stability. Low physiological dose choline supplementation recapitulates many structural, functional, and molecular benefits observed with GSO, including attenuation of fibrosis, preservation of myocardial deformation, improved systolic performance, and prevention of bioenergetic decline. Our data suggest that GSO and choline converge on several candidate pathways by dampening pro-hypertrophic RAF/MEK/ERK signaling, normalizing calcium handling, and partially restoring actomyosin ATPase driven contractility, thereby implicating a choline centered metabolic signaling axis in HF induced by pressure overload. Choline thus emerges as a principal, though not yet definitively proven, mediator of the cardioprotective actions of GSO. Priority future work includes: (1) mechanistic validation of the identified pathways through targeted molecular perturbation; (2) comprehensive profiling of GSO's bioactive landscape to identify synergistic components; (3) Safety assessments of oral choline supplementation regarding metabolic byproducts (e.g., TMAO); and (4) translational validation across diverse HF phenotypes and human-relevant platforms. These efforts will help bridge the gap from mechanistic discovery to the development of GSO-based or choline-centered therapeutic strategies for heart failure.

Funding

This research was supported by grants from the Guangdong Basic and Applied Basic Research Foundation (Grant Nos. 2024A1515010959, 2023A1515011278, 2022A1515012338, 2022A1515011154, and 2023A1515011278) and the Key Technologies Research and Development Program of Guangdong Province (Grant No. 2008A08003).

Reference

[1] S.S. Martin, A.W. Aday, Z.I. Almarzooq, et al., 2024 Heart Disease and Stroke Statistics: A Report of US and Global Data From the American Heart Association, Circulation. 149 (2024) e347-e913. https://doi.org/10.1161/cir.0000000000001209.

[2] K.T. Mills, J.D. Bundy, T.N. Kelly, et al., Global Disparities of Hypertension Prevalence and Control: A Systematic Analysis of Population-Based Studies From 90 Countries, Circulation. 134 (2016) 441-450. https://doi.org/10.1161/circulationaha.115.018912.

[3] E.D. Frohlich, C. Apstein, A.V. Chobanian, et al., The heart in hypertension, N Engl J Med. 327 (1992) 998-1008. https://doi.org/10.1056/nejm199210013271406.

[4] K.L. Peterson, Pressure overload hypertrophy and congestive heart failure. Where is the "Achilles' heel"?, J Am Coll Cardiol. 39 (2002) 672-675. https://doi.org/10.1016/s0735-1097(01)01790-9.

[5] F.H. Messerli, S.F. Rimoldi, S. Bangalore, The Transition From Hypertension to Heart Failure: Contemporary Update, JACC Heart Fail. 5 (2017) 543-551. https://doi.org/10.1016/j.jchf.2017.04.012.

[6] X. Li, W. Tan, S. Zheng, et al., Differential mRNA expression and circRNA-based ceRNA networks in the three stages of heart failure in TAC mice, Front. Physiol. . (2022) 777284. https://doi.org/10.3389/fphys.2022.777284.

[7] M.S. Madhur, F. Elijovich, M.R. Alexander, et al., Hypertension: Do Inflammation and Immunity Hold the Key to Solving this Epidemic?, Circ Res. 128 (2021) 908-933. https://doi.org/10.1161/circresaha.121.318052.

[8] F. Kuwahara, H. Kai, K. Tokuda, et al., Hypertensive myocardial fibrosis and diastolic dysfunction: another model of inflammation?, Hypertension. 43 (2004) 739-745. https://doi.org/10.1161/01.HYP.0000118584.33350.7d.

[9] S. Chakraborty, J. Mandal, T. Yang, et al., Metabolites and Hypertension: Insights into Hypertension as a Metabolic Disorder: 2019 Harriet Dustan Award, Hypertension. 75 (2020) 1386-1396. https://doi.org/10.1161/hypertensionaha.120.13896.

[10] M.M. Salvatore, A. Elvetico, M. Gallo, et al., Fatty Acids from Ganoderma lucidum Spores: Extraction, Identification and Quantification, Applied Sciences. 10 (2020) 3907. https://www.mdpi.com/2076-3417/10/11/3907

[11] B.S. Min, N. Nakamura, H. Miyashiro, et al., Triterpenes from the spores of Ganoderma lucidum and their inhibitory activity against HIV-1 protease, Chem Pharm Bull (Tokyo). 46 (1998) 1607-1612. https://doi.org/10.1248/cpb.46.1607.

[12] X. Bao, C. Liu, J. Fang, et al., Structural and immunological studies of a major polysaccharide from spores of Ganoderma lucidum (Fr.) Karst, Carbohydr Res. 332 (2001) 67-74. https://doi.org/10.1016/s0008-6215(01)00075-1.

[13] S.Y. Lee, H.M. Rhee, Cardiovascular effects of mycelium extract of Ganoderma lucidum: inhibition of sympathetic outflow as a mechanism of its hypotensive action, Chem Pharm Bull (Tokyo). 38 (1990) 1359-1364. https://doi.org/10.1248/cpb.38.1359.

[14] O.B. Shevelev, A.A. Seryapina, E.L. Zavjalov, et al., Hypotensive and neurometabolic effects of intragastric Reishi (Ganoderma lucidum) administration in hypertensive ISIAH rat strain, Phytomedicine. 41 (2018) 1-6. https://doi.org/10.1016/j.phymed.2018.01.013.

[15] Y. Kabir, S. Kimura, T. Tamura, Dietary effect of Ganoderma lucidum mushroom on blood pressure and lipid levels in spontaneously hypertensive rats (SHR), J Nutr Sci Vitaminol (Tokyo). 34 (1988) 433-438. https://doi.org/10.3177/jnsv.34.433.

[16] Y.Z. Xie, F. Yang, W. Tan, et al., The anti-cancer components of Ganoderma lucidum possesses cardiovascular protective effect by regulating circular RNA expression, Oncoscience. 3 (2016) 203-207. https://doi.org/10.18632/oncoscience.316.

[17] P. Lai, X. Cao, Q. Xu, et al., Ganoderma lucidum spore ethanol extract attenuates atherosclerosis by regulating lipid metabolism via upregulation of liver X receptor alpha, Pharm Biol. 58 (2020) 760-770. https://doi.org/10.1080/13880209.2020.1798471.

[18] Y. Liu, G. Lai, Y. Guo, et al., Protective effect of Ganoderma lucidum spore extract in trimethylamine-N-oxide-induced cardiac dysfunction in rats, J Food Sci. 86 (2021) 546-562. https://doi.org/10.1111/1750-3841.15575.

[19] N.P. Sudheesh, T.A. Ajith, K.K. Janardhanan, Ganoderma lucidum (Fr.) P. Karst enhances activities of heart mitochondrial enzymes and respiratory chain complexes in the aged rat, Biogerontology. 10 (2009) 627-636. https://doi.org/10.1007/s10522-008-9208-9.

[20] A.A. da Silva, J.M. do Carmo, X. Li, et al., Role of Hyperinsulinemia and Insulin Resistance in Hypertension: Metabolic Syndrome Revisited, Can J Cardiol. 36 (2020) 671-682. https://doi.org/10.1016/j.cjca.2020.02.066.

[21] G. Jia, J.R. Sowers, Hypertension in Diabetes: An Update of Basic Mechanisms and Clinical Disease, Hypertension. 78 (2021) 1197-1205. https://doi.org/10.1161/hypertensionaha.121.17981.

[22] R. Zhou, M. Yang, C. Yue, et al., Association between Dietary Choline Intake and Cardiovascular Diseases: National Health and Nutrition Examination Survey 2011-2016, Nutrients. 15 (2023) https://doi.org/10.3390/nu15184036.

[23] P.M. Ueland, Choline and betaine in health and disease, J Inherit Metab Dis. 34 (2011) 3-15. https://doi.org/10.1007/s10545-010-9088-4.

[24] A.A. Strilakou, A.C. Lazaris, A.I. Perelas, et al., Heart dysfunction induced by choline-deficiency in adult rats: the protective role of L-carnitine, Eur J Pharmacol. 709 (2013) 20-27. https://doi.org/10.1016/j.ejphar.2013.03.025.

[25] M. Kocaturk, Z. Yilmaz, M. Cansev, et al., Choline or CDP-choline restores hypotension and improves myocardial and respiratory functions in dogs with experimentally - Induced endotoxic shock, Res Vet Sci. 141 (2021) 116-128. https://doi.org/10.1016/j.rvsc.2021.10.010.

[26] S.H. Zeisel, M. Warrier, Trimethylamine N-Oxide, the Microbiome, and Heart and Kidney Disease, Annu Rev Nutr. 37 (2017) 157-181. https://doi.org/10.1146/annurev-nutr-071816-064732.

[27] X. Li, W. Tan, S. Zheng, et al., Cardioprotective Effects of n-3 Polyunsaturated Fatty Acids: Orchestration of mRNA Expression, Protein Phosphorylation, and Lipid Metabolism in Pressure Overload Hearts, Frontiers in Cardiovascular Medicine. 8 (2022) https://doi.org/10.3389/fcvm.2021.788270.

[28] R. Ram, D.M. Mickelsen, C. Theodoropoulos, et al., New approaches in small animal echocardiography: imaging the sounds of silence, Am J Physiol Heart Circ Physiol. 301 (2011) H1765-1780. https://doi.org/10.1152/ajpheart.00559.2011.

[29] S. Zheng, W. Tan, X. Li, et al., Apelin receptor inhibition in ischemia-reperfused mouse hearts protected by endogenous n-3 polyunsaturated fatty acids, Frontiers in Pharmacology. 14 (2023) https://doi.org/10.3389/fphar.2023.1145413.

[30] X. Li, S. Zheng, W. Tan, et al., Slit2 Protects Hearts Against Ischemia-Reperfusion Injury by Inhibiting Inflammatory Responses and Maintaining Myofilament Contractile Properties, Front Physiol. 11 (2020) 228. https://doi.org/10.3389/fphys.2020.00228.

[31] S. Zheng, W. Tan, X. Li, et al., Aged Monkeys Fed a High-Fat/High-Sugar Diet Recapitulate Metabolic Disorders and Cardiac Contractile Dysfunction, J Cardiovasc Transl Res. 14 (2021) 799-815. https://doi.org/10.1007/s12265-021-10105-z.

[32] F.H. Yang, W.G. Pyle, Reduced cardiac CapZ protein protects hearts against acute ischemia-reperfusion injury and enhances preconditioning, J Mol Cell Cardiol. 52 (2012) 761-772. https://doi.org/10.1016/j.yjmcc.2011.11.013.

[33] F. Yang, D.L. Aiello, W.G. Pyle, Cardiac myofilament regulation by protein phosphatase type 1alpha and CapZ, Biochem Cell Biol. 86 (2008) 70-78. https://doi.org/10.1139/o07-150.

[34] E.W. Hancock, B.J. Deal, D.M. Mirvis, et al., AHA/ACCF/HRS recommendations for the standardization and interpretation of the electrocardiogram: part V: electrocardiogram changes associated with cardiac chamber hypertrophy: a scientific statement from the American Heart Association Electrocardiography and Arrhythmias Committee, Council on Clinical Cardiology; the American College of Cardiology Foundation; and the Heart Rhythm Society. Endorsed by the International Society for Computerized Electrocardiology, J Am Coll Cardiol. 53 (2009) 992-1002. https://doi.org/10.1016/j.jacc.2008.12.015.

[35] D. Levy, R.J. Garrison, D.D. Savage, et al., Prognostic implications of echocardiographically determined left ventricular mass in the Framingham Heart Study, N Engl J Med. 322 (1990) 1561-1566. https://doi.org/10.1056/nejm199005313222203.

[36] R.B. Devereux, B. Dahlöf, E. Gerdts, et al., Regression of hypertensive left ventricular hypertrophy by losartan compared with atenolol: the Losartan Intervention for Endpoint Reduction in Hypertension (LIFE) trial, Circulation. 110 (2004) 1456-1462. https://doi.org/10.1161/01.Cir.0000141573.44737.5a.

[37] J. Chan, L. Deng, L.G. Mikael, et al., Low dietary choline and low dietary riboflavin during pregnancy influence reproductive outcomes and heart development in mice, Am J Clin Nutr. 91 (2010) 1035-1043. https://doi.org/10.3945/ajcn.2009.28754.

[38] M. Xu, R.Q. Xue, Y. Lu, et al., Choline ameliorates cardiac hypertrophy by regulating metabolic remodelling and UPRmt through SIRT3-AMPK pathway, Cardiovasc Res. 115 (2019) 530-545. https://doi.org/10.1093/cvr/cvy217.

[39] L. Liu, Y. Lu, X. Bi, et al., Choline ameliorates cardiovascular damage by improving vagal activity and inhibiting the inflammatory response in spontaneously hypertensive rats, Sci Rep. 7 (2017) 42553. https://doi.org/10.1038/srep42553.

[40]D.A. Eisner, J.L. Caldwell, K. Kistamás, et al., Calcium and Excitation-Contraction Coupling in the Heart, Circ Res. 121 (2017) 181-195. https://doi.org/10.1161/circresaha.117.310230.

[41] D.M. Bers, Calcium cycling and signaling in cardiac myocytes, Annu Rev Physiol. 70 (2008) 23-49. https://doi.org/10.1146/annurev.physiol.70.113006.100455.

[42] S. Rouhana, C. Farah, J. Roy, et al., Early calcium handling imbalance in pressure overload-induced heart failure with nearly normal left ventricular ejection fraction, Biochim Biophys Acta Mol Basis Dis. 1865 (2019) 230-242. https://doi.org/10.1016/j.bbadis.2018.08.005.

[43] F.H. Yang, W.G. Pyle, Cardiac actin capping protein reduction and protein kinase C inhibition maintain myofilament function during cardioplegic arrest, Cell Physiol Biochem. 27 (2011) 263-272. https://doi.org/10.1159/000327952.

[44] D.R. Van Wagoner, A.L. Pond, P.M. McCarthy, et al., Outward K+ current densities and Kv1.5 expression are reduced in chronic human atrial fibrillation, Circ Res. 80 (1997) 772-781. https://doi.org/10.1161/01.res.80.6.772.

[45] T.M. Olson, A.E. Alekseev, X.K. Liu, et al., Kv1.5 channelopathy due to KCNA5 loss-of-function mutation causes human atrial fibrillation, Hum Mol Genet. 15 (2006) 2185-2191. https://doi.org/10.1093/hmg/ddl143.

[46] R. Coppini, C. Ferrantini, NaV1.8: a novel contributor to cardiac arrhythmogenesis in heart failure, Cardiovasc Res. 114 (2018) 1691-1693. https://doi.org/10.1093/cvr/cvy210.

[47] P. Facer, P.P. Punjabi, A. Abrari, et al., Localisation of SCN10A gene product Na(v)1.8 and novel pain-related ion channels in human heart, Int Heart J. 52 (2011) 146-152. https://doi.org/10.1536/ihj.52.146.

[48] N. Dybkova, S. Ahmad, S. Pabel, et al., Differential regulation of sodium channels as a novel proarrhythmic mechanism in the human failing heart, Cardiovasc Res. 114 (2018) 1728-1737. https://doi.org/10.1093/cvr/cvy152.

[49] Z.J. Lu, A. Pereverzev, H.L. Liu, et al., Arrhythmia in isolated prenatal hearts after ablation of the Cav2.3 (alpha1E) subunit of voltage-gated Ca2+ channels, Cell Physiol Biochem. 14 (2004) 11-22. https://doi.org/10.1159/000076922.

[50] C.L. Huang, Murine Electrophysiological Models of Cardiac Arrhythmogenesis, Physiol Rev. 97 (2017) 283-409. https://doi.org/10.1152/physrev.00007.2016.

[51] C.J. Liang, C.W. Lee, H.C. Sung, et al., Ganoderma lucidum Polysaccharides Reduce Lipopolysaccharide-Induced Interleukin-1 β Expression in Cultured Smooth Muscle Cells and in Thoracic Aortas in Mice, Evid Based Complement Alternat Med. 2014 (2014) 305149. https://doi.org/10.1155/2014/305149.

[52] C. Zhen, X. Wu, J. Zhang, et al., Ganoderma lucidum polysaccharides attenuates pressure-overload-induced pathological cardiac hypertrophy, Front Pharmacol. 14 (2023) 1127123. https://doi.org/10.3389/fphar.2023.1127123.

[53] F. Xu, X. Li, X. Xiao, et al., Effects of Ganoderma lucidum polysaccharides against doxorubicin-induced cardiotoxicity, Biomed Pharmacother. 95 (2017) 504-512. https://doi.org/10.1016/j.biopha.2017.08.118.

[54] J. He, Y. Sun, Y. Jia, et al., Ganoderma triterpenes Protect Against Hyperhomocysteinemia Induced Endothelial-Mesenchymal Transition via TGF-β Signaling Inhibition, Front Physiol. 10 (2019) 192. https://doi.org/10.3389/fphys.2019.00192.

[55] R. Mukherjee, F.G. Spinale, L-type calcium channel abundance and function with cardiac hypertrophy and failure: a review, J Mol Cell Cardiol. 30 (1998) 1899-1916. https://doi.org/10.1006/jmcc.1998.0755.

[56] S. Engelhardt, L. Hein, F. Wiesmann, et al., Progressive hypertrophy and heart failure in beta1-adrenergic receptor transgenic mice, Proc Natl Acad Sci U S A. 96 (1999) 7059-7064. https://doi.org/10.1073/pnas.96.12.7059.